Thermographic Image Analysis as a Pre-Screening Tool for the Detection of Canine Bone Cancer

By Samrat Subedi, Bachelor of Science

A Thesis Submitted in Partial

Fulfillment of the Requirements

for the Degree of

Master of Science

in the field of Electrical and Computer Engineering

Advisory Committee:

Scott E. Umbaugh, Chair

Robert LeAnder

Bradley Noble

Graduate School
Southern Illinois University Edwardsville
December, 2014

ABSTRACT

THERMOGRAPHIC IMAGE ANALYSIS AS A PRE-SCREENING TOOL FOR THE DETECTION OF CANINE BONE CANCER

by

SAMRAT SUBEDI

Chairperson: Professor Dr. Scott E. Umbaugh

Introduction: Bone cancer is a common type of cancer in canines. There are different types of bone cancer of which osteosarcoma is the most common corresponding to more than 90% of all tumors in large breed dogs. It usually appears in the limbs and grows fast and is highly metastatic. Imaging methods such as x-ray, computed tomography (CT), magnetic resonance imaging (MRI), and biopsy are used primarily for diagnosing this disease. These medical imaging techniques are most prevalent and are being extensively used in diagnostic imaging, but they are not suitable as a pre-screening method due to some disadvantages; including high expense, high dose of radiation, and keeping the patient (canine) motionless during the imaging procedures. Also this type cancer has high metastatic potential and may not be diagnosed using these techniques before it has spread to other body parts.

Objectives: This research study explores the possibility of using thermographic images as a pre-screening tool for diagnosis of bone cancer in dogs, the advantages include being non invasive, cheaper, faster, no radiation, real time imaging, portable and available for computer aided image analysis.

Experimental Methods: Experiments were performed in several stages with different sample sizes and combinations of images. Research started by dividing all the images into two groups, cancer and no-cancer. Results were analyzed and further divisions of

images were made based on body parts, hair type, and body area and then more experiments were conducted. These experiments were analyzed to identify how images should be divided to improve the results. All the experiments were performed with color normalization using temperature data provided by the Long Island Veterinary Specialists. After analyzing the initial experimental results it was determined that grouping by separate body parts provided better results than with other division of images. For this the images were first divided into four groups according to body parts (Elbow/Knee, Full Limb, Shoulder/Hip and Wrist). Each of the groups was then further divided into three sub-groups according to views (Anterior, Lateral and Posterior). Thermographic patterns of normal and abnormal dogs were analyzed using feature extraction and pattern classification tools. Texture features, spectral feature and histogram features were extracted from the thermograms and were used for pattern classification. Three different pattern classification tools, CVIP-FEPC, Partek Discovery Suite and Artificial Neural Network were used to classify the thermograms.

Results: The best classification success rate in canine bone cancer detection was 90% with sensitivity of 100% and specificity of 80% produced by anterior view of full-limb region with nearest neighbor classification method and normRGB-lum color normalization method with CVIP-FEPC as pattern classification tool. Three experiments with each data normalization method that provide best result for each experimental setup were chosen and were used for Partek Discovery Suite. Only those features that were used on those experiments were considered. Nearest neighbor along with discrimininant analysis were used as pattern classification tools. The result was almost same as the one obtained from CVIP-FEPC in some case one or two samples being misclassified. This shows that the pattern classification algorithms that were used in CVIP-FEPC were sufficient for pattern classification for this research. The features extracted using CVIP-FEPC were then used to classify images using an artificial neural network using Matlab. The feature values that were not normalized were used. Principal component transform was used before these were input to the artificial neural network. Only the principal components that contain 98% of the variance were considered. The best classification success rate of 100% with 100% sensitivity and 100% specificity was obtained for

anterior view of full limb region with artificial neural network as the pattern classification method.

Conclusion: Our results show that it is possible to use thermographic imaging as a pre-screening tool for detection of canine bone cancer. We have also determined that separation of images considering factors like body parts, camera view, body area making a homogeneous data set has significant effect on the success rate.

ACKNOWLEDGEMENTS

First of all I would like to thank my parents and my entire family members for their love and support.

I am heartily thankful to my advisor Dr. Scott Umbaugh for believing in me and giving me opportunities to be involved in his research lab from the first day of school. The encouragement and support at every stage of this research study I got from him is incomparable. I want to express my appreciation for my master's committee members, Dr Bradley Noble and Dr. Robert LeAnder for their valuable feedback and support. I would like to express my appreciation to all the members of Computer Vision and Image Processing Laboratory, SIUE. I am also grateful to Terrill Smith for all the help, support he gave to me. I am so much thankful to Heema and Krishna for the love and care they provided me every day. I would also like to thank all my friends of Maryville, who were there to help me through the toughest time. I am also grateful to the Long Island Veterinary Specialists for providing thermographic images and funding for this research project

TABLE OF CONTENTS

LIST OF FIGURES

LIST OF TABLES

CHAPTER 1

INTRODUCTION

1.1 Motivation and Background

Bone cancer is one of the common diseases in dogs. Among different types of tumors osteosarcoma is most common in middle aged to older dogs primarily in large breeds like Saint Bernards, Great Danes, Rottweilers, Golden Retrievers, Irish Setters, Labrador Retrievers, and Doberman Pinschers. Osteosarcoma (osteo = bone, sarcoma = cancer) which can occur in any body part but appear primarily in the limbs, is called "appendicular osteosarcomas" and is very aggressive, so will spread to other parts very fast [1]. The nature of this kind of cancer is that the tumors grow from the inside outward and destroy the bone from inside out. A common symptom is lameness after one to three months after first swelling is seen. The bone with tumor is not strong and breaks with slight injury and never heals. These fractures confirm the diagnosis of bone cancer and are commonly called "pathologic fractures".

The main problem with this kind of cancer is its symptoms are similar to other common problems. In most cases these symptoms are treated for other medical problems such as sprains, joint injuries and arthritis. Symptoms like acute pain are seen when the cancer has already spread to other parts of the body. Medical imaging is a vital part in diagnosis, monitoring the disease and treatment that includes planning potential surgical procedures. Analysis of radiography, MRI and biopsy are being largely used in for the detection of bone cancer. All of these techniques provide information about the anatomic information but they are not well suited for preliminary diagnostic of disease both logistically and economically.

Radiography has always been the first choice for orthopedic related disease, the drawback being its high radiation. MRI produces excellent images from soft tissue to bone. This makes MRI the first choice for diagnosing internal medical problems. The problem of using MRI as a pre-screening tool is the cost and inconvenience. Another major problem is the necessity of sedation as animals cannot stay on an MRI machine for 30 to 40 minutes in a standstill position. In a biopsy, the actual cells from the body are taken and are examined by medical personnel. Biopsy is not a good choice as a pre-screening tool.

Due to its potential metastasis, even when the tumor is detected using these methods, it has already spread to other body parts. This indicates the necessity of early detection of cancer so that treatment can be started as early as possible. Here we explore the use of infrared thermography as a tool for the preliminary detection of bone cancer in dogs. The main advantage of this technique is sedation is not necessary to perform the screening and the changes in the thermographic patterns can be seen before they are actually confirmed using clinical signs and radiographic abnormalities [2, 3]. The other advantages of thermography include: portability, real time imaging which makes it useful for a computer based application, and non-contact, so it is hygienic and non-invasive in nature. Evaluation of thermograms has been used since the 1960s but mostly manually, the result being highly dependent on human subjectivity. In this research we study the use of thermographic images as a pre-screening tool for the detection of bone cancer in canines. Computer based image analysis and data analysis tools have been developed and used for this research study.

1.2 Objective of the Thesis

The main objective of this thesis work is to investigate the possibility of using thermographic image analysis methods as a pre-screening tool for canine bone cancer. Specifics are as follows:

1. Classify the thermographic images as normal or abnormal based on features extracted from the image.

2. Investigate the possibility of using Artificial Neural Networks as a pattern classification tool in classification of thermographic images.

3. Determine which camera view, body parts, and color normalization method provides the best result.

4. Determine which set of features, data normalization methods, and pattern classification algorithms are optimal in classification of thermographic images for this application.

5. Create a base on which more research can be performed with other algorithms and approaches.

1.3 Thesis Structure

The thesis is organized into six different chapters.

Chapter 1 provides motivation, background and objectives of this research study.

Chapter 2 provides an introduction to canine bone cancer, medical imaging systems and previous related works.

Chapter 3 provides a description of material and tools that have been used in this research.

Chapter 4 explains the methodology used for this research study which includes a detailed explanation of the algorithm followed to conduct this research.

Chapter 5 provides all the experimental results and discussion.

Chapter 6 concludes the overall research with possible future work.

CHAPTER 2
LITERATURE REVIEW

2.1 Bone Cancer in Dogs

Bone cancer in dogs is a fatal disease. There are primarily four types of tumors which are: osteosarcoma, chondrosarcoma, fibrosarcoma, and hemangiosarcoma. The most common type of cancer is osteosarcoma which accounts for 98% of bone tumors [2]. It has been estimated that every year there are 10,000 dogs affected by this disease in the US alone. Although it can occur in any dog, it is more prevalent in older large breeds of dogs. This type of cancer is aggressively painful and rapidly spreads to other organs through the blood stream. The exact cause of this type of cancer is yet unknown but repetitive bone injury, previous bone disease, viral infection, radiation, and genetic disease are the most common explanations as the causes of cancer. The wrist, knee, shoulder or hip are the most common areas where this cancer is found, however it can occur in other body parts as well. The figure below shows the common sites where this cancer is primarily found which are distal femur and proximal tibia which we called as elbow/knee region, distal radius which we called as wrist region and proximal humerus which we called as shoulder/hip region.

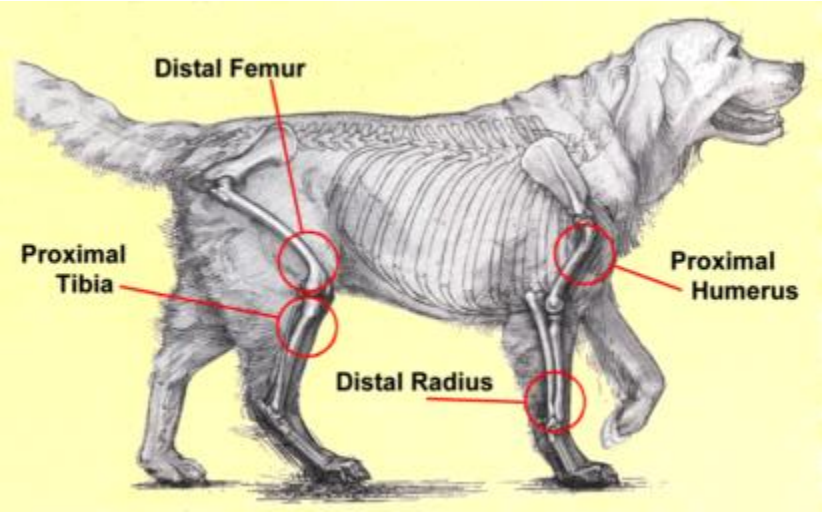

Figure 1: Common sites for osteosarcoma development in canine.
(Source: http://www.marvistavet.com/html/body_canine_osteosarcoma.html)

2.1.1 Clinical symptoms, diagnosis and treatment

Osteosarcoma has a high metastatic potential that can cause cancer to spread to other parts of body before symptoms are observed. In most dogs it cannot be seen during first diagnosis and almost 90% of clinically diagnosed cancer has already metastasized. The nature of this type of cancer is it develops in the inner part of the bone and destroys the bone from inside to the outside.

There are no specific symptoms associated with bone cancer. But the most common sign is lameness, crying due to pain and swelling. Though symptoms like loss of weight, loss of appetite, irritability, restlessness, and aggression are not directly associated with bone cancer, they may occur due to the high degree of pain and discomfort. The cancer makes the bone so weak that it breaks with slight injury which is another symptom of bone cancer. There are various treatment procedures available which are limb-sparing surgery, palliative radiation therapy, bisphosphonates, samarium–153, and amputation. The treatment highly recommended for this type of cancer is the amputation of the affected leg which will not highly affect the day to day functionality of the dog. With amputation, the primary tumor is removed and spreading of cancer to other organs is prevented and it also removes the pain caused by the primary tumor. But if the cancer has already spread to other parts of body then other techniques are used to reduce the pain. In some cases multiple procedures are also applied such as chemotherapy with amputation which will increase survival time. In most cases the cause of death is due to the spread of the cancer, primarily to the lungs, so even after the treatment the survival time is six months to a maximum of one year because of its high metastatic potential. [3].

Early detection and early treatment is necessary to prolong the life of the dog. In most cases the symptoms of bone cancer are common to other problems such as joint problems, sprains, arthritis and medication for pain relief, anti-inflammatories are given which actually lessen the symptoms. As this kind of cancer is most common in middle aged to older dogs of larger breeds, it is always better to find the disease sooner than before the actual symptoms are observed.

2.2 Medical Imaging System

Medical imaging systems are used to acquire information about physiological characteristics of humans or animals. There are different types of imaging systems currently being used in the medical field for diagnosing canine bone cancer. These imaging methods are used for evaluation of the disease and also for evaluation of metastasis.

2.2.1 Radiography

In general radiography is used to produce a static image of the internal structure of body. X-rays are used, which when passed through the body will be partially absorbed, partially scattered and the rest passed through towards the detector. The amount of x-ray absorbed is different for different body parts, for example, tissue absorbs less x-ray than bones. The x-ray that passed though the body is recorded and produced on films.

Figure 2: X-ray of dog limb with osteosarcoma.
(Source: http://www.osteosarcomaindogs.org/what-is-dog-osteosarcoma/)

Radiography is often used for diagnosing orthopedic related disease. X-rays are primarily used for detection of canine bone cancer as it destroys the bone thus making changes which can be seen on x-ray films. However, other diseases such as bone injury, or infection may also produce a similar radiograph. In most cases an x-ray of lungs is also taken to check

metastases. The other problem associated with the x-ray is it requires 30% to 50% change in bone minerals compared to normal bones which makes it insensitive to small lesions [4]. Although x-rays are the first choice in diagnostic imaging, high exposure to x-ray radiation is not good for the animal's health and may cause radiation induced cancer.

2.2.2 Computerized Tomography (CT)

Computerized Tomography (CT) combines the medical imaging system with a computer. With CT it is possible to display x-ray images in cross section and also possible to generate images of a single slice of body. With the advancement in technology, now it is possible to represent different anatomic component with different colors. Though CT produces images with most details, they also require a high dose of radiation. In order to double the resolution without increasing pixel noise, the level of radiation should be increased by 16 times [5]. Due to this, CT is being highly used for diagnosing many different kinds of internal medical problems. The advantage of using CT for bone cancer is it can be used to image soft tissues, bones, blood vessels and also for lung metastases. Due to the high level of radiation, cost associated, and complex imaging procedure CT is not a good choice as a pre-screening method.

2.2.3 Magnetic Resonance Imaging (MRI)

Magnetic Resonance Imaging (MRI) is considered as one of the best medical imaging techniques due to its high image resolution, possibility of acquiring images from any plane, excellent soft tissue contrast and no ionizing radiation. Magnetic resonance is a phenomenon where charge particles with angular and magnetic moment in magnetic field absorb or emit electromagnetic energy [5]. The moment that is associated with charge particles in motion is the basics behind MRI. When a strong magnetic field is formed around the subject, the free hydrogen nuclei align with the direction of magnetic field. The nuclear moment is than detected using radio frequency. With bountiful advantages, MRI possesses few limitations that prevent it from being first choice as a pre-screening tool which include cost and the time required to take MRI images.

2.2.4 Infrared Thermography

Infrared thermography is a non-invasive, quantitative assessment of temperature, producing a color image called a thermogram that represents the surface temperature of an object. This medical imaging system is different than other systems as it does not use the energy from the imaging source. Plank's radiation law states that any object above absolute temperature emits radiation. The radiation power and the distribution is given by Planks radiation law [6].

$$W(\lambda, T) = \frac{2\Pi hc^2}{\lambda^4}\left[exp\left(\frac{hc}{\lambda kT}\right) - 1\right]^{-1} Wcm^{-2}\mu m^{-1} \quad (1)$$

Where,

h is plank's constant =6.6256 X 10^{-34} Js
c is velocity of light=2.9979 X 10^{8} m/s
k is boltzman's constant =1.38054 X 10^{-23}WsK^{-1}
ƛ is wavelength in μm
T is temperature in K

Infrared energy is a part of the electromagnetic spectrum that is invisible to the human eye and hence we perceive it as heat. So a thermographic image is a display of the temperature distribution profile from the subject using different colors to represent different temperatures. The temperature that is measured on the surface is not the heat conducted from the internal body and hence is the function of the sympathetic nervous system. As this heat is not from the internal body, it is not affected by the heat of deeper parts. The local temperature is however affected by disease or injuries which cause local dermal microcirculation to vary [7]. Thermography is useful because of its sensitivity to pathology in the vascular, muscular, neural and skeletal systems. The correlation between the surface temperature recording with disease or injury is the clinical basis of thermography. The increase or decrease in the amount of infrared radiation from body is indicated by the spectrum of colors. For a normal body there is high degree of thermal symmetry and hence any change in temperature asymmetry represents abnormality.

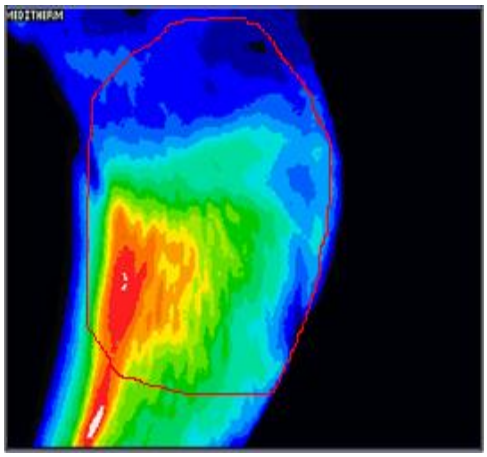

Figure 3: Thermographic images of elbow of a dog with bone cancer, red circle indicating the area of interest

The pattern of the color map represents the heat gradient with white or red regions being the most hot and blue or black are the coolest regions. The advantages of thermography include the possibility of diagnosis, evaluation, monitoring and documenting a large number of injuries and conditions, including soft tissue injuries and sensory/autonomic nerve fiber dysfunction. Due to its advantages such as non invasive in nature, no radiation, fast and economic procedure, thermography is a good choice as a pre-screening tool.

2.3 Related Works

Use of temperature as a health indicator has been widespread in the medical arena for the past five decades [8]. The usefulness of thermograms for diagnosing different physical illness was verified by Barnes in 1963 [9]. Though criticized as a false positive generator, use of thermography has been proven valuable for diagnosing several problems in animal as well as human medicine. Jung et al. showed how infrared thermography can be used in medical applications [10]. A.L Schaefer et al. used thermographic along with RFID for automatic detection of bovine respiratory disease [11]. Sloveig M. Stubjoen et al. studied the possibility of detecting the pain in ship due to various problems using the changes in eye temperature using infrared themography along with heart rate variability [12]. Stewart M. et al. studied the effect of stress on eye temperature using thermographic images in dairy cattle [13]. Infrared thermography has been proved valuable for diagnosing spinal cord injury in dogs [14]. Use of thermography has been used in animal like horses,, llamas, and cattle [15-23].

Infrared thermography has also been used in human medicine for diagnosis of breast cancer [24-29], burn patients [24], joint disease [30], vascular disorder [31], pnemothorax [32], intervetibral disk disease [33], lumbar disc herniation, peripheral neuropathy, cardiovascular disease [34-38], and bowel ischemia [39]. Bob Berry et al. proposed a method where thermography was used along with ultrasonic device, 3D camera and dermatascope for early detection of diabetes mellitus [40]. The possibility of thermograms for the detection of carpal tunnel syndrome has been studied has been proved as a promising method [41]. The usefulness of themography in sports as a pre-scanning tool for athletes to evaluate overuse and traumatic knee injuries has been studied and was recommended [42]. Nikola Borojevic et al. investigates on possibility of using thermography as a method to differentiate healthy joints with rheumatoid arthritis and osteoartheritics and concludes that there are significant difference in the temperature distribution among different kind of thermograoms [43]. A. Merla et al. highlight the importance of infrared imaging in diagnostic imaging [44]. The use of infrared imaging in various medical applications has been reviewed by Ring et al. [45].

The use of thermography in breast cancer detection has been widely explored with more than 800 peer-reviewed studies [46]. The use of thermography for breast cancer detection has always been a topic for debate among researchers. After the approval from the FDA as an adjunctive diagnostic screening procedure for breast cancer detection in 1982, many research studies were done in this area. The use of thermography has been widely used for early breast cancer detection [47-51].

Most of the research associated with analysis of thermograms uses classical analysis of thermograms. With the advance in technology, cameras with higher thermal resolution, and spatial resolutions are available. This requires advanced analysis of thermographic images using computer technology. Analysis of thermograms using advanced quantitative statistic analysis has been present in [52, 53]. Qi H. et al proposed a method to analyze thermal system with analogy with electrical circuit theory [54]. Use of artificial neural networks for pattern classification have been widely explored. Harold Szu et al. used a neural network for the early detection of breast cancer [55]. J. Koay et al. present a method that analyzes the asymmetry between contra lateral breasts using a back propagation trained artificial neural network [56]. Hairong Qi et al. present an approach to analyze the asymmetry in human

breasts using automatic segmentation and pattern classification. Use of artificial neural network methods have been recommended for analyzing thermograms [57-62]

CHAPTER 3
MATERIALS AND TOOLS

Various types of tools and materials were used during this research to determine whether thermographic image analysis can be used as a pre-screening tool for evaluating thermographic images of bone cancer in canines. Software tools were used in algorithm development and hardware tools to capture the thermographic images of the canines.

3.1 Experimental Animals

The images were taken from both healthy limbs as well as cancerous limbs confirmed using biopsies regardless of sex, breed, hair types and age. For most of the cases one limb is affected by cancer most of which were osteosarcoma. So the opposite limb of the same dog was considered as no-cancer limb making the number of cancerous images almost same as no cancer images. These thermographic images were taken at the laboratory of the Long Island Veterinary Specialists (LIVS). Initial research used images from 34 dogs; more images were added as the research progressed making total number of dogs 41 for final studies.

3.2 Digital Infrared Thermal Imaging System

The digital infrared thermal imaging (DITI) system used is the Meditherm Med2000 IRIS, which is based on clinical requirements and is designed for medical applications. This system has an accuracy of 0.01° C and can measure temperature from 10° C - 55° C. The thermograms generated are TIFF images with a choice of six palettes in full color, isotherm or grayscale. The system is capable of focusing to small areas down to 75 × 75mm. The program was preset for a temperature range of 8°C with a 16 shade color map [63]. The warmer regions were represented by white and red colors while the cooler regions were represented by black and blue colors. The image of the ROI will be focused and image taken will later be adjusted in temperature scale of 8°C range.

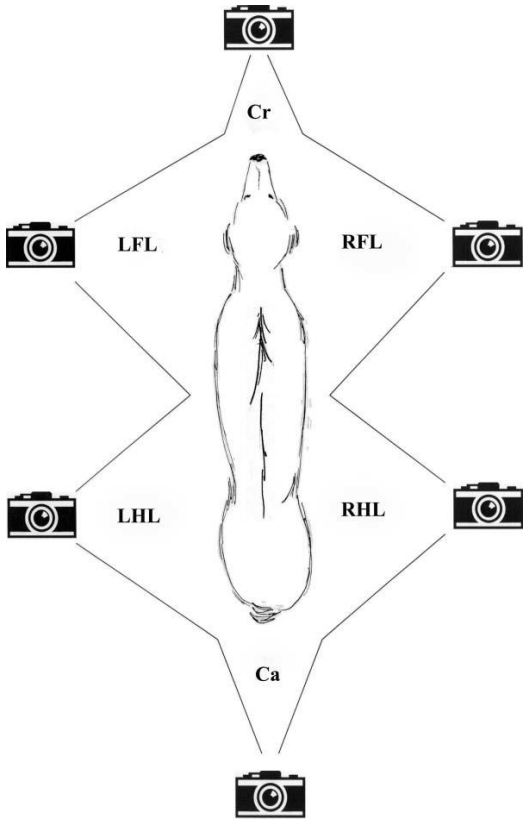

Figure 4: Figure showing the different camera position while taking thermographic images [7].

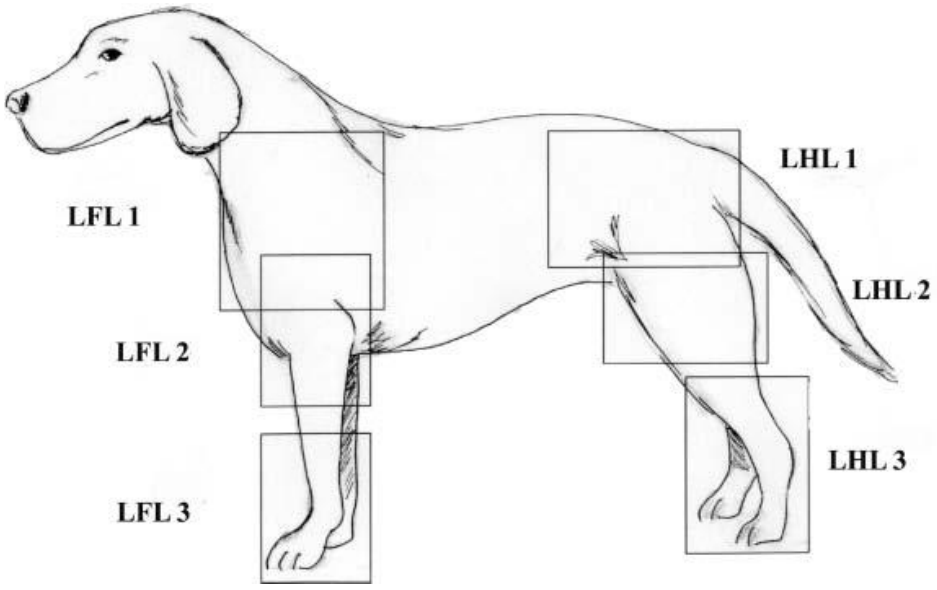

Figure 5: Position of dog during thermography showing different position of limb from left side (LHL = left hind limb, LFL= left front limb) [64].

3.3 Thermographic Images

All the images used in this research were obtained from the LIVS. For each dog thermographic images were taken from different views, in a temperature controlled room at 21°C. Latex gloves were used by the technician to hold the animal for positioning to prevent thermal artifacts from manual contact. The camera position was typically 1.5 to 4.6 meters from the dogs depending on camera view. The maximum temperature, minimum temperature and average temperature for the region of interest were also noted for each image taken. Images from 34 dogs were considered at the initial phase of this research. Further experiments were done with 39 and 41 dogs. Images were taken from four different views which were anterior taken from front, lateral taken from side, posterior taken from back and medial which is opposite to lateral and taken from inside to out.

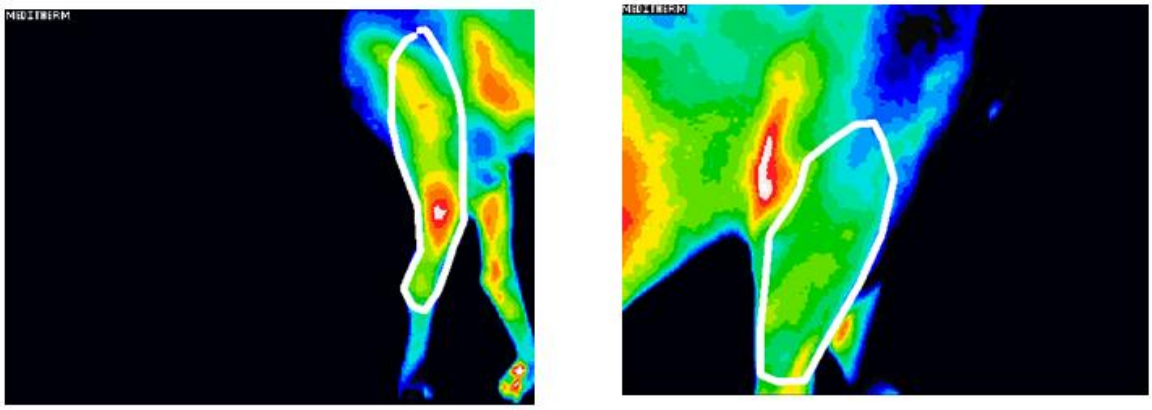

Figure 6: Thermographic image of normal right hind limb with indicated ROI (left) and cancerous left hind limb (right) of same dog.

3.4 Software Tools Used

Different software tools have been utilized for this research study which includes the SIUE computer vision and image processing tools (CVIPtools), Computer vision and image processing feature extraction and pattern classification (CVIP-FEPC) and color normalization software that were developed at Computer Vision and Image Processing (CVIP) laboratory of Southern Illinois University at Edwardsville (SIUE). Other tools used

were Partek Discovery Suite, Matlab 2012, Microsoft Visual Studio 2010 and Microsoft Excel.

3.4.1 Computer Vision and Image Processing Tools (CVIPtools)

CVIPtools is free software developed to work with Windows. It is an excellent, interactive program for image processing and computer vision application development. CVIPtools consists of standard image processing functions such as image compression, image restoration, logical and arithmetical operations, contrast manipulation, image sharpening, frequency transforms, edge detection, segmentation and geometric transformations [65]. CVIPtools also contains two powerful development tools that allow for batch processing and automatic algorithm analysis and development. CVIPtools was used in this research primarily for creating the border masks. It was also used to convert the feature files obtain from CVIP-FEPC to Microsoft Excel format.

3.4.2 Feature Extraction and Pattern Classification (CVIP-FEPC)

CVIP-FEPC is a tool developed primarily for feature extraction and pattern classification. It provides both feature extraction and pattern classification in a single run. This software allows the user to select different combinations of features to be extracted from a large group of images. Automatically, after feature extraction of all images, a combination of pattern classification methods selected by the user is implemented. Finally, the software produces a total correctness classification rate, and also the classification rate for each class, by which the sensitivity, and specificity of each set of experiment can be calculated.

3.4.3 Color Normalization Software

The color normalization software remaps the thermographic images based on the temperature data. The software was written using Microsoft C#. It maps the images into four different types which are lum, normGrey, normRGB and normRGB-lum [66].

3.4.4 Partek Discovery Suite

The Partek Discovery Suite is a statistical and visualization tool that is most useful for finding patterns in the data [67]. It consists of a number of data analysis and visualization

tools that help to easily solve a wide range of pattern analysis and pattern recognition problems. Partek Discovery Suite was used for performing principal component transform and also for pattern classification purpose.

3.4.5 Matlab

Matlab is a high level language and environment to analyze data, develop algorithms, and create models [68]. With a large number of built in functions, matlab can be used to solve many kinds of engineering problems. In this research study, matlab was used for performing the pattern classification using ANN.

CHAPTER 4
METHODOLOGY

This research study uses a series of operations to fulfill the objectives. Different tools and software were used to perform different operations which are described below.

4.1 Mask Creation

The primary purpose of the mask is to extract the region of interest (ROI). The masks for individual thermographic images were created using CVIPtools based on the region of interest determined by the veterinary specialist. Once the mask is overlapped with the image, only the area of interest is left for further analysis.

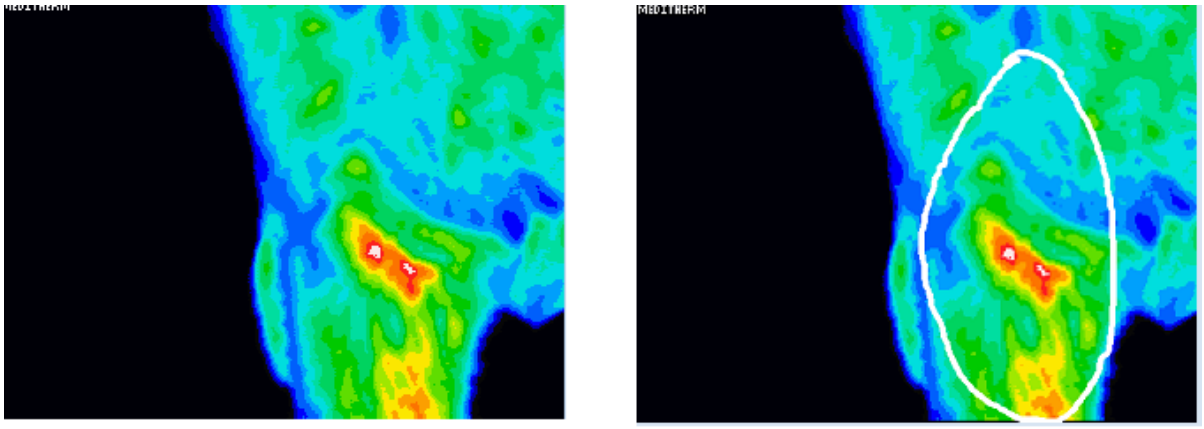

Figure 7: Original thermographic image (left), and image with indicated ROI (right)

The above figure shows the mask creation steps. The left image is the thermographic image taken using the thermographic camera. The second image specifies the ROI. Based on the second image a mask is created which is shown in figure 8. When the mask is overlapped with the thermographic images, only the part of the image that falls on the white area will be present and rest of the image will be black as shown by the images below on the right.

Figure 8: Manual mask created using CVIPtools (left) and image obtained after overlapping with mask (right).

4.2 Color Normalization

The specific colors in the thermographic images depends on the palette that is chosen with the imaging software while taking the images. So the same color may not represent same temperature all the time. Different color pallets can be chosen to represent the temperature distribution and perception on those images might be different. For color normalization the thermograms were remapped based on the maximum and minimum temperatures of the experimental set. Four different color normalization mappings, Luminance, Norm-Grey, Norm-RGB and Norm-RGB-Lum were used and obtained using the software developed at the SIUE CVIP research lab [66]. The reason behind the use of color normalization is to take account of varying camera settings during image acquisition. This means one color may represent different temperatures in different images depending upon the camera settings, which are adjusted by the operator to maximize the visual information.

The Lum method, which actually performs no color normalization by itself, is to generate a grey image from the color image using the linear equation

$$Grey\ Level = 0.3 * Red + 0.6 * Green + 0.1 * Blue \quad (2)$$

The Norm-Grey method maps the minimum and maximum temperature to the grey level range of 0 to 255. The pixel value of resultant image represents the pixel's temperature of the corresponding original image. The Norm-RGB method works the same way as

normGrey, but it uses color palette. The Norm-RGB-lum method is obtained after applying Norm-RGB method followed by lum [66].

Figure 9: Color normalized thermographic image of normal right hind limb (from left to right Luminance, Norm-Grey, Norm-RGB, and Norm-RGB-Lum).

Color normalization for this research was done separately for normal and abnormal image sets. Results from combining the normal and abnormal images before color normalization can be found in Appendix B.

4.3 Feature Selection and Extraction

To analyze the temperature distribution pattern of the thermograms, different image features were extracted from the images. Three primary feature types were selected for this research which includes texture features, histogram features, and spectral features.

4.3.1 Texture features

Texture is a function of image size and magnification of images and is related to properties like smoothness, coarseness and roughness [70]. The second order histogram of the grey levels based on the joint probability distribution has been used to measure the texture. The statistics based on the pairs of pixel and their grey level can be obtained using the second order histogram, also called the grey level co-occurrence matrix. The two parameters distance and angle are the basis of these texture features. The distance specifies the distance between the pairs of pixels and the angle specifies the angle between them. A pixel distance of seven was used for this research as this value produced better result and found experimentally. Different features can be extracted with these methods but only five different features were considered for this research which was available in CVIP-FEPC.

For a given distance and angle, the texture features are calculated as below [70].

$$\text{Energy} = \sum_i \sum_j c_{ij}^2 \quad (3)$$

$$\text{Inertia} = \sum_i \sum_j (i-j)^2 c_{ij} \quad (4)$$

$$\text{Inverse Difference} = \sum_i \sum_j \frac{c_{ij}}{|i-j|} \text{ ; for } i \neq j \quad (5)$$

$$\text{Entropy} = -\sum_i \sum_j c_{ij} \log_2 c_{ij} \quad (6)$$

$$\text{Correlation} = \frac{1}{\sigma_x \sigma_y} \sum_i \sum_j (i-\mu_x)(j-\mu_y) c_{ij} \quad (7)$$

Where

c_{ij} are elements in the co-occurrence matrix normalized by dividing by the number of pixel pairs in the matrix.

$$\mu_x = \sum_i i \sum_j c_{ij}$$

$$\mu_y = \sum_j j \sum_i c_{ij}$$

$$\sigma_x^2 = \sum_i (i-\mu_x)^2 \sum_j c_{ij}$$

$$\sigma_y^2 = \sum_j (j-\mu_y)^2 \sum_i c_{ij}$$

Average and range for texture features were extracted for this research study.

4.3.2 Histogram features

The histogram provides information about the image grey level distribution and is basically a plot between numbers of pixel at each gray level value versus the gray levels. The histogram features were calculated after modeling the histogram as probability distribution of gray level. The histogram features are extracted for each RGB color band for color images.

Histogram features includes mean, standard deviation, skew and entropy. These features are calculated using following equations [70].

$$Mean(\bar{g}) = \sum_{g=0}^{L-1} gP(g) \quad (8)$$

Where $P(g) = \frac{N(g)}{M}$ is first order histogram probability, M is number of pixel in the image, N(g) is number of pixel at grey level g , L is total number of grey level.

$$\text{Standard Deviation}(\sigma_g) = \sqrt{\sum_{g=0}^{L-1}(g - \bar{g})^2 P(g)} \quad (9)$$

$$\text{Skew} = \frac{1}{\sigma_g^3}\sum_{g=0}^{L-1}(g - \bar{g})^3 P(g) \quad (10)$$

$$\text{Energy} = \sum_{g=0}^{L-1}[P(g)]^2 \quad (11)$$

$$\text{Entropy} = -\sum_{g=0}^{L-1} P(g)\log_2[P(g)] \quad (12)$$

The histogram features were calculated for each of the three RGB color band for color images.

4.3.3 Spectral features

Spectral features are frequency domain based features where power is the primary metric. Power in various regions is calculated for spectral features, where region being box, ring or sector. The spectral power in certain area can be calculated using the following equation [70].

$$Spectral\ Region\ Power = \sum_{u \in REGION} \sum_{v \in REGION} |T(u,v)|^2$$

Spectral features are also useful for obtaining texture information as regions with high power in low frequencies corresponds to coarse textures. In a similar manner fine textures have high power in high frequencies.

Spectral features for three rings and sectors were calculated for this research study. For color images these features were calculated for each color band separately. Besides this, three

spectral DC values were also calculated for each color band for color images and one for monochromatic images.

Eleven features were thus used in this research which includes; spectral, five texture features, and five histogram features. The spectral features were measured for three rings and three sectors for each RGB color band, so six values for monochrome images and 18 for color. Additionally, the spectral feature also includes the average DC values for each RGB color band. Note that in the software the spectral feature values were treated as one feature, even though they had multiple values. The texture features include texture energy, inertia, correlation, inverse difference and entropy. Average and range values were extracted for all these texture features. Five histogram features were calculated for all color bands. With all these features there were 46 different feature values that were extracted for each thermogram. For original images histogram mean features were not extracted because they are not normalized and so there were only 43 feature values. For monochromatic images, feature values from a single band were extracted. The table below shows all the features that were extracted from non monochromatic thermographic images.

Table 1: Features extracted from thermograms using CVIP-FEPC for color image.

Histogram Features	Texture Features	Spectral Features
Histogram Mean R Band*	Texture Energy Average	Spectral DC R Band
Histogram Mean G Band*	Texture Energy Range	Ring 1 R Band
Histogram Mean B Band*	Inertia Average	Ring 2 R Band
Histogram Standard Deviation R Band	Inertia Range	Ring 3 R Band
Histogram Standard Deviation G Band	Correlation Average	Sector 1 R Band
Histogram Standard Deviation B Band	Correlation Range	Sector 2 R Band
Histogram Skew R Band	Inverse Difference Avg.	Sector 3 R Band
Histogram Skew G Band	Inverse Difference Range	Spectral DC G Band
Histogram Skew B Band	Texture Entropy Average	Ring 1 G Band
Histogram Energy R Band	Texture Entropy Range	Ring 2 G Band
Histogram Energy G Band		Ring 3 G Band
Histogram Energy B Band		Sector 1 G Band
Histogram Entropy R Band		Sector 2 G Band
Histogram Entropy G Band		Sector 3 G Band
Histogram Entropy B Band		Spectral DC B Band
		Ring 1 B Band
		Ring 2 B Band
*Not Extracted for original images		Ring 3 B Band
		Sector 1 B Band
		Sector 2 B Band
		Sector 3 B Band

CVIP-FEPC was used to extract the features which provide a text file which used further to be used by pattern classification tools such as Partek and Matlab.

4.4 Data Normalization

Data normalization is necessary before pattern classification as the range of different components of feature vectors varies vastly. So it is necessary to put all the data in similar ranges so they all have equal importance for the pattern classification. Two data normalization methods were used to normalize the extracted feature data which were standard normal density normalization and softmax scaling with r=1[70] as these were found to be useful for this kind of research problems [71,72].

4.4.1 Standard normal density

Standard normal density is one of the common statistical based methods. For normalization the mean is first calculated and then subtracted from each feature and then divided by standard deviation to obtain the new feature which is in the range of 0 to 1. The mathematical explanation for this data normalization can be explained as below [70].

Considering k feature vectors $F_j = \{F_1, F_2, \dots, F_k\}$ having n features in each vector

$$F_j = \begin{bmatrix} f_{1j} \\ f_{2j} \\ \vdots \\ \cdot \\ \cdot \\ f_{nj} \end{bmatrix} \text{ for j= 1,2,…,n}$$

The new set of vectors is calculated as

$$f_{ijSND} = \frac{f_{ij} - m_i}{\sigma_i} \quad for\ all\ i,j$$

Where

Mean $m_i = \frac{1}{k}\sum_{j=1}^{k} f_{ij} \quad for\ i = 1,2,\dots,n$

And standard deviation $\sigma_i = \sqrt{\frac{1}{k}\sum_{j=1}^{k}(f_{ij} - m_i)^2} \qquad For\ i = 1,2,\dots,n$

4.4.2 Softmax scaling

Softmax scaling compresses data into the range of 0 to 1 and is one of the non linear normalization methods. The normalization is done in two steps [70].

At first data are mapped similar to standard normal density

$$y = \frac{f_{ij} - m_i}{r\sigma_i}$$

Where m_i is mean, f_{ij} is feature vector, σ_i is standard deviation and r is user defined factor

The normalized data is then obtained using the following equation

$f_{ij_{SMC}} = \frac{1}{1+e^{-y}}$ for all i,j

4.5 Pattern Classification

In image analysis pattern classification is used to classify images based on the extracted feature values. For this an algorithm is necessary which uses the information from the features. In order to develop a pattern classification algorithm, the images are first divided into two sets, a training set which is used to develop the algorithm and a test set which is used to test the algorithm. The images in both sets should be complete and should contain images from the entire domain. Three different pattern classification software tools were used during this research: CVIP-FEPC, Partek Discovey Suite and Matlab. CVIP-FEPC was used as a pattern classification tool for the initial experiments. Partek Discovery Suite and Matlab were also used along with CVIP-FEPC for later experiments.

4.5.1 CVIP-FEPC as a pattern classification tool

CVIP-FEPC consists of different classification methods which include nearest neighbor, K-nearest neighbor and nearest centroid. The result from CVIP-FEPC not only provides the best classification success rate but it also provides the most important feature sets that were used for pattern classification. The output from CVIP-FEPC provides the results of all

experiments and this is helpful for selecting the best features for future experiments. Leave one out testing was used where all but one images are used as the training set and the test is performed on the one that was left out. This process is repeated for all the samples. The success rate is calculated by number of images that are classified correctly. For this research study pattern classification was performed using nearest neighbor and K-nearest neighbor with k=5 methods.

4.5.2 Nearest neighbor

Nearest neighbor is the simplest pattern classification algorithm where the test sample is compared to every sample in the training set using a distance measure, a similarity measure, or combination of both. If a distance metric is used, it looks for smallest distance measured between object of interest feature vector and other feature vectors of samples in the training set. This algorithm is not robust and is also computationally intensive.

4.5.3 K-nearest neighbor

K-nearest neighbor in a manner similar to nearest neighbor is based on closest training samples in the feature space. In this method not only the single closest sample but group of close feature vectors are considered. The number of samples to be considered is determined by value of K. If k=1 it is nearest neighbor classification.

4.5.4 Distance and similarity measure

Distance measure and similarity measures are used to compare two feature vectors n for classification. Distance metrics measure the difference between two vectors and similarity measure measures their closeness. If they have a small difference or a large similarity, those two are considered from same class. Various metrics are used to measure the distance and similarity; for example euclidean distance, city block, absolute value, vector inner product, correlation coefficient.

For this research study Euclidean distance was used as the metric for measuring distance. For two feature vectors X and Y with vector components, the euclidean distance can be calculated using the following equation [70].

$$d_E(X,Y) = \sqrt{\sum_{i=1}^{n}(x_i - y_i)^2}$$

4.5.5 Success measure

A success measure is necessary to check how accurate the classification algorithm is. The number of samples classified correctly or incorrectly can be the simplest success measure, however this cannot be used as the only criteria for evaluation. The cost and risk associated with misclassification are also important. Two other metrics, sensitivity and specificity were used along with the average success rate.

Sensitivity is the success rate for the disease class, and is represented as

$$Sensitivity = \frac{TP}{TP + FN}$$

Specificity is the success rate for the "no disease" class, given that the subject does not have disease and is represented as

$$Specificity = \frac{TN}{TN + FP}$$

Where

TP (True Positive) = correctly classified positive, disease present cases
TN (True Negative) = correctly classified negative, disease absent cases
FP (False Positive) = incorrectly classified negative cases
FN (False Negative) = incorrectly classified positive cases

4.5.6 Partek Discovery Suite as a pattern classification tool

The Partek Discovery Suite has various tools that can be used for classification: discriminant analysis and multi-layer perception, which is a specific type of ANN [67].

4.5.7 Model selection

The purpose of selecting a model is to define which variable to use, how many variables to use, what classification algorithm to use, selection of distance and similarity measure and selection of validation method. For each classification algorithm chosen, the software generates a model with the selected variables, distance and similarity measures. The variables in model selection refers to features values extracted using CVIP-FEPC. The features that were used for best classification in CVIP-FEPC were chosen. Two pattern classification methods, K-nearest neighbor with value of k = 1, 3 and 5, and discriminant analysis were used. Euclidean distance was used as distance measure metric and overall classification success rate along with sensitivity and specificity were used as success measures.

4.5.8 Discriminant analysis

Discriminant analysis is used to determine the possibility of classification of a set of objects into predefined classes. It is necessary to define objects into different classes before developing the model, referred to as supervised classification. Two types of discriminant functions are available in Partek, linear and quadratic, and both were used for this research study. Partek also has the option for two types of prior probabilities, equal and proportional, both of which were used for this research study.

Linear discriminant analysis uses linear functions to separate the classes where a set of linear discriminant functions is calculated from the common covariance matrix and within-group means. Quadratic discriminant analysis uses quadratic functions to separate classes where the set of quadratic discriminant functions is calculated from within group covariance matrices and the within group means. In both cases these functions are used to partition the feature space into different class regions.

4.5.9 Artificial Neural Network as a pattern classification tool

An artificial neural network (ANN) consists of interconnected processors called neurons. These neurons can be related as neurons in the brain. A neuron receives numbers of inputs and produces more than one output. Neurons are connected with other neurons by weighted links that pass the signal from one neuron to another. Weights are basically the memory of ANN which is adjusted periodically called learning of neural network. Once an ANN is trained, it generates the output with new set of input data.

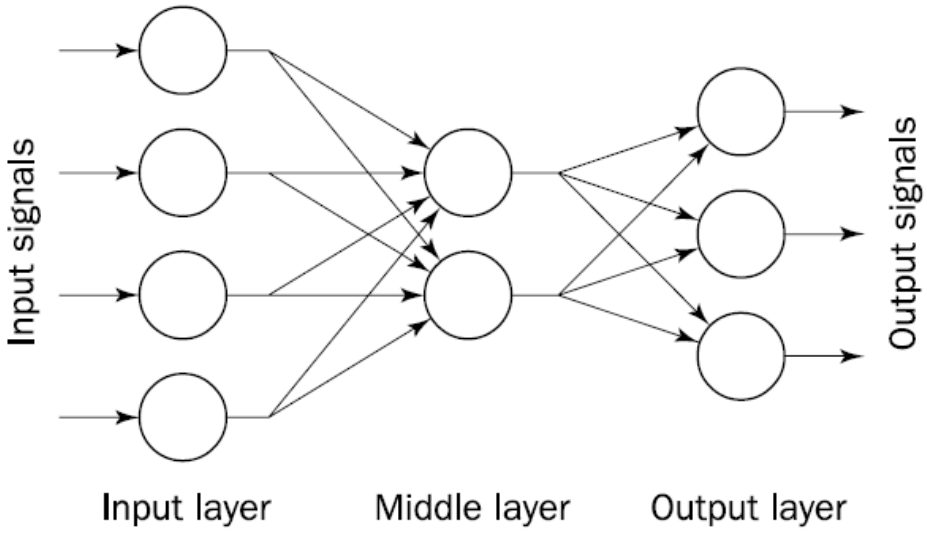

Figure 10: Architecture of a typical artificial neural network

4.5.10 Backpropagation algorithm

The backpropagation algorithm is a training algorithm based on supervised learning. This means the network should have prior knowledge of desired results. The operation of the backpropagation algorithm starts with providing the inputs through input layers. The weights are initially set in between +1 to -1 [68]. The hidden layers process the input and provide the output from output layer. As the network already knows the output, error is calculated which is the difference between actual output and desired output. This error is then propagated back to network and based on the error the weights of the network are adjusted. This process is repeated until specified error value is reached. A back propagation algorithm is ideal choice

for pattern recognition task [69]. The neural network toolbox available in Matlab was used in this research for pattern classification.

4.5.11 Network design

Network design includes: design of input data, selection of various variables for the network, selection of algorithms for training the network, and evaluation of the success measures.

4.5.12 Selection of input features

Preprocessing on feature data obtained from CVIP_FEPC was done using the principal component transform available in the Partek Discovery Suite before input to the network.

Principal Component Analysis (PCA) is a technique to analyze the data in which data are described by numbers of inter-correlated quantitative dependent variables. The main objective of PCA is to extract the information that is most important and represent them as a new set called principal components and rank them according to their importance. Principal component analysis is a linear transformation that converts original variables to new variables.

PCA can also be thought as principal axis rotation of the original variables where the total variance is preserved. The rotation and variation is defined by eigenvectors and eigenvalues. The correlation method was used for this research study, which adjust the data to be zero mean and standard deviation of one. The reason behind selecting this method was the ranges of input variables, feature vectors, were not uniform. The inputs to the networks, which are the principal components of feature vectors, were arranged as a column in matrix and target vector was set either to 0 or 1. A sample matrix is shown below. The sample input matrix contains the samples which are the thermographic images as column and principal components of features as row. The sample target class separate each sample in one of two classes, value 1 in any class represents that the sample being in that class.

	Sample 1	Sample 2	Sample 3	Sample n
PC1	1.32652	0.103109	-0.68623	6.08837
PC2	2.02853	0.962357	1.4328	-6.58303
PC3	1.23236	-0.98647	0.81233	-7.4004
PC4	1.39736	1.14914	-2.1453	-0.81988
PC5	-0.81031	1.95565	0.232942	-5.21231
PC6	0.168523	0.909466	0.690899	1.89506

Figure 11: Sample input matrix for the neural network.

	Sample 1	Sample 2	Sample 3	Sample n
class 1	1	0	0	1
class 2	0	1	1	0

Figure 12: Sample target class matrix for neural network.

4.5.13 Training and testing of network

The training data was divided into three subgroups called training, validation and test sets. The training data are used to update the network weight. The validation subset is used to monitor the training process. When the training is started, the training error and validation error are both high and start to decrease as training progresses. The validation error starts to increase after certain epochs which is considered as over fitting. The network at minimum validation error is considered an optimal network.

The test subset is not used during training and validation but is used to see the test error for different models. Seventy percent of data were used as training, 20% for validation and 10% for test. These division was made randomly using Matlab inbuilt function *dividerand*. The network was designed with 10 hidden layers, feed forward with sigmoid transfer function at both hidden layer and output layer. Among the different training algorithms available in Matlab, the scaled conjugate gradient (SCG) algorithm was used for training algorithm. The parameters used by SCG can be found in [68]. The performance of the network was

calculated using cross entropy which calculates the network performance with given targets, outputs, and performance weights [68]. The default derivative was used which calculates and returns Jacobian errors. Two plots were used to evaluate the network viz. confusion plot and receiver output characteristics curve. The network was trained again and again until acceptable plots were not achieved which means low error and high success rate.

4.6 Experimental Methods

The flowchart shown below explains the overall steps followed for this research study.

Two sets of images were obtained from LIVS, one set thermographic image and another with the ROI indicated by the veterinary specialist. The images were at first divided into different groups. CVIPtools was used to create the manual mask based on the ROI indicated. After a mask is created color normalization was performed using the color normalization software developed at SIUE. The software was written using Microsoft C# and it uses the temperature data of all the images provided by LIVS. The temperature data sheet was prepared manually which contains the name of the dog, maximum temperature, minimum temperature and average temperature. The software outputs five folders with masks for the original and the four color normalized images. The CVIP-FEPC software was then used for feature extraction and pattern classification. This software has specially designed for running multiple experiments by selecting multiple features, data normalization methods and pattern classification methods. The result of FEPC consists of three different files: 1) summary file, 2) feature file and 3) individual experiment result files. Sample of these files are included in appendix A. The summary file gives the classification success rate for each experiment along with the important features used for classification purpose. The feature file contains all the feature values extracted from all the images which can be used as input for other pattern classification tools. The individual experiment result file contains the details of each experiment along with sensitivity and specificity. These results were then analyzed to determine the overall success rate, sensitivity, specificity, useful feature sets and classification method that provide the best result.

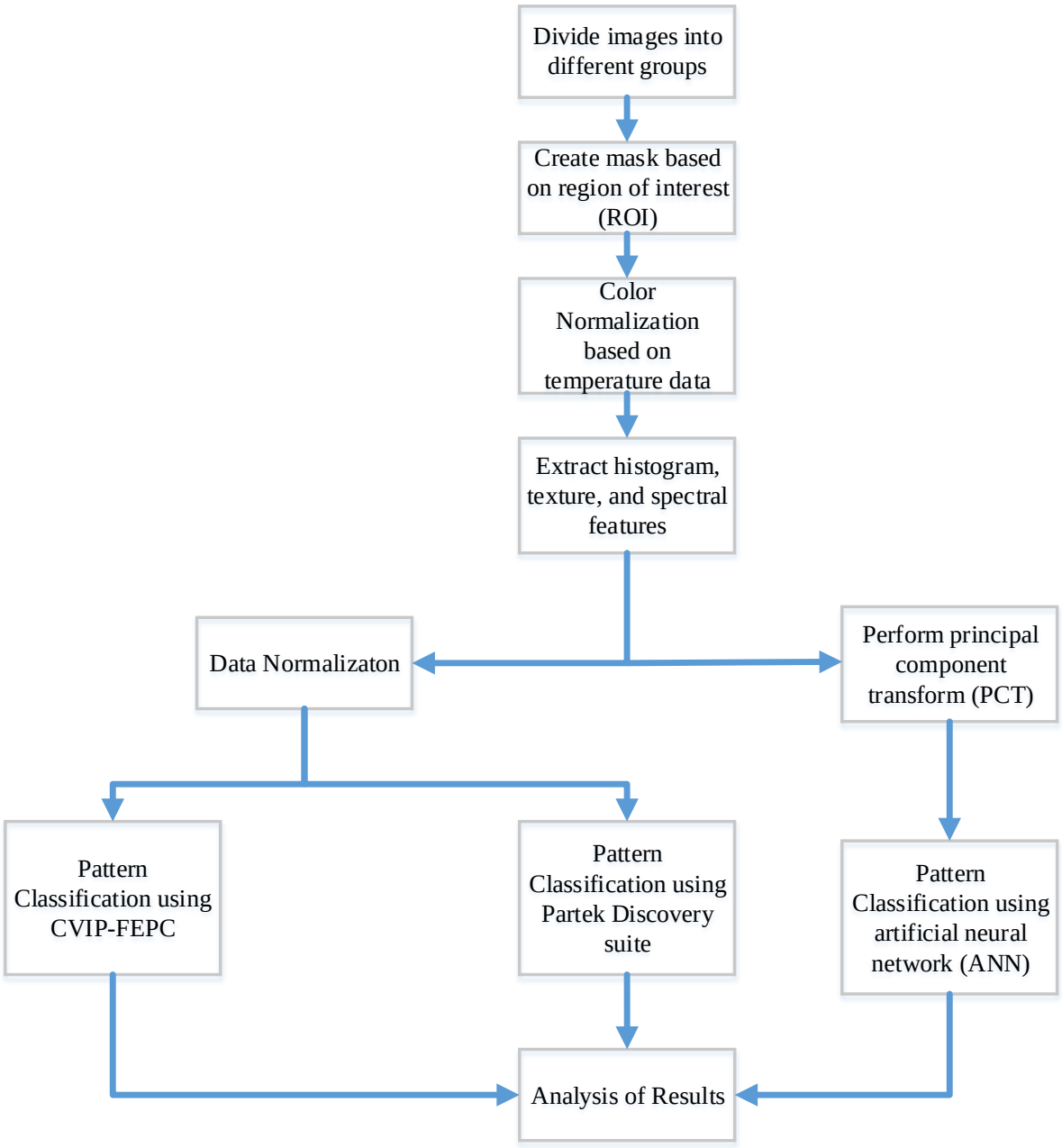

Figure 13: Flowchart showing all the steps performed for overall research

The feature files obtained from CVIP FEPC were also used for pattern classification using the Partek Discovery Suite. The experiments that generate best result for each data normalization method in CVIP-FEPC were chosen to be used for Partek. Only those features that were used for best classification on those experiments were used in Partek. Based on the

features selected, pattern classification methods chosen and distance and similarity measure chosen, Partek generate a model and run the experiment with all possible combinations. After the completion of experiment Partek provide a complete report of model selection based on which different success measure can be calculated. A sample report from Partek is included in Appendix A

The other classification method used in this research was the artificial neural network. Principal component analysis was performed to decorrelate and normalize the data before inputting to the neural network. The principal components feature values were chosen such that the total variance is greater than 98%. The Partek Discovery Suite was used to perform the PCA. Covariance method was chosen that operate on mean centered data. During the computation of the covariance matrix, the data is automatically mean centered [67]. In order to use artificial neural networks, the images were randomly divided into two sets, training set and test set. The network was designed using matlab and was trained using training set. Once the network was trained, test set was used to test the network. The successfulness of network was evaluated using success measures which include overall success rate, sensitivity and specificity.

CHAPTER 5
RESULT AND DISCUSSION

This research study used thermographic images of healthy as well as cancerous limbs of dogs and the efficacy of classifying images with image analysis methods was investigated. The research work was conducted in a series of four stages.

5.1 First Stage of Experiment

In the first stage, all the images were divided into two groups, cancer and no-cancer that include images of all the body parts and camera views. The research was started with images from 34 dogs of which 140 were from cancerous limbs and 141 from no-cancer limbs. Five set of experiments were performed using CVIP-FEPC for original as well as four different color normalized groups. The color normalization was performed separately for normal and abnormal group throughout this research study. Texture features with texture pixel distance of 6, histogram features and spectral features were extracted from the thermographic images. Two data normalization methods, standard normal density and softmax scaling and two pattern classification methods, nearest neighbor and K nearest neighbor with K=5 was used. The table below shows the best result of five experimental set with original and different color normalization method for all the body parts.

Table 2: Table showing the overall success rate, sensitivity and specificity with all the body parts and camera view combined

Body Part	Color Normalization	Success Rate	Sensitivity	Specificity
All Limb 34 Dogs cancer: 140 no-cancer: 141	Original	59.07%	62.41%	55.71%
	Lum	64.06%	63.12%	65.00%
	NormGrey	61.21%	51.06 %	51.43%
	NormRGB	61.21%	49.65%	54.29%
	NormRGB-lum	62.28%	52.48%	60.71%

The table shows a poor result with highest classification success rate being 64.06% with sensitivity of 63.12% and specificity of 65.00%. The reason behind the poor results could be because the images were from different tissue types, body parts, camera view, gender and breeds. This indicates that images should be divided considering these factors before going for further analysis. The results from color normalization set is higher compared to original image set thus signifying the continuation of color normalization for further experiments.

Table 3: Features, data normalization and pattern classification methods used for best classification.

Body Part	Color Normalization	Features	Data Normalization	Pattern Classification
All Limb 34 Dogs cancer: 140 no-cancer: 141	Original	Spectral Texture Inertia Texture Correlation Texture Entropy Histogram Skew Histogram Entropy	Soft-max, r = 1	KNN5
	Lum	Texture Entropy Histogram StdDev Histogram Energy	none	KNN5
	NormGrey	Texture Correlation Histogram Mean Histogram StdDev Histogram Skew	Soft-max, r = 1	KNN5
	NormRGB	Texture Energy Texture Entropy Histogram Mean Histogram Energy Histogram Entropy	Standard Normal	KNN5
	NormRGB-lum	Texture Correlation Texture Entropy Histogram Skew Histogram Entropy	Soft-max, r = 1	KNN5

The features, data normalization method and pattern classification method used for the experiments that produce best classification success rate for original and color normalization methods are shown above. This is useful for analyzing which features, pattern classification and data normalization methods were more useful than other.

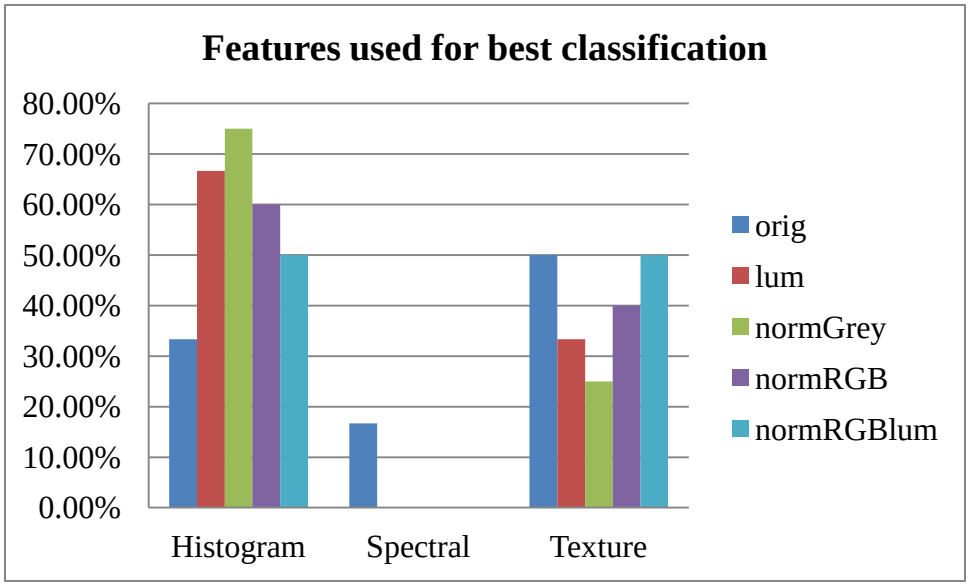

Figure 14: Features used by original and color normalized set for best classification success.

The bar diagram shown above shows which features were mostly used for best classification. This shows that spectral feature was only used for original image set. The bar diagram also shows the importance of texture and histogram features for the classification. A complete division of features and their occurrence is shown by following figure.

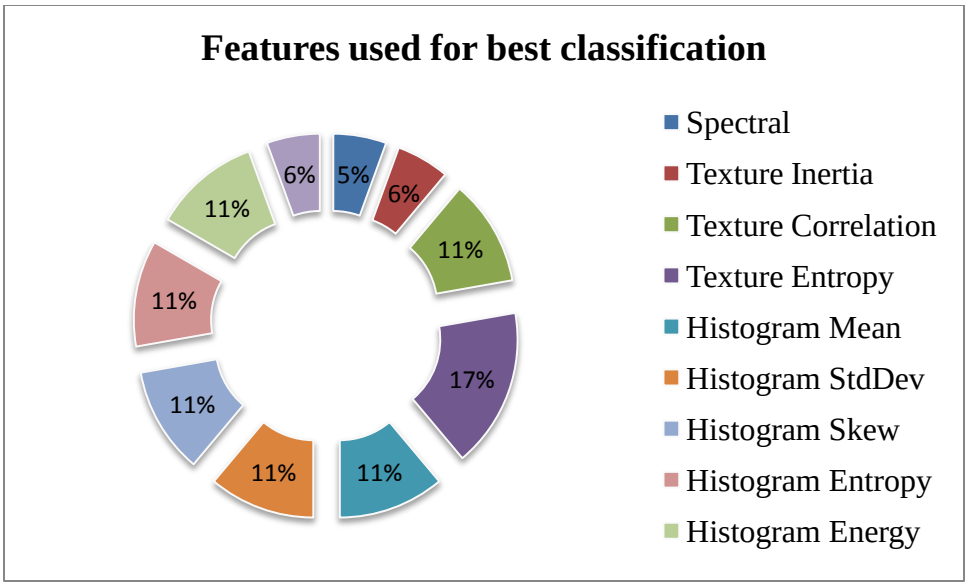

Figure 15: Features used for best classification for all experiments

The pie chart above shows that texture entropy was mostly used for pattern classification by the experiments that produce best result. On the other hand texture energy, texture inertia and spectral features were least used for pattern classification.

5.2 Second Stage of Experiment

At the initial part of this stage we only had samples from 34 dogs; later we had images from 39 dogs. Since the result obtained from first stage of experiment was not impressive, at this stage we ran experiments dividing images into different groups based on the hair type, body parts, limb type, and body area. Division based on gender and breed was not performed due to insufficient data sets.

At first, the images were divided into four groups based on different body parts viz. elbow/Knee, full limb, shoulder/hip and wrist. The same features, data normalization methods and pattern classification methods that were used in first stage of experiment were used here. The following tables show the best results for four different body parts with original as well as color normalized groups.

Table 4: Classification results for elbow/knee region.

Body Part	Color Normalization	Success Rate	Sensitivity	Specificity
Elbow Knee With 34 Dogs cancer: 66 non-cancer: 67	Original	61.94%	70.59%	53.03%
	Lum	64.92%	61.76%	68.18%
	NormGrey	62.68%	63.02 %	70.55%
	NormRGB	60.15%	55.88%	64.62%
	NormRGB-lum	63.15%	63.24%	63.08%

Table 5: Classification results for full limb region.

Body Part	Color Normalization	Success Rate	Sensitivity	Specificity
Full Limb With 34 Dogs cancer: 18 non-cancer: 19	Original	62.16%.	57.89%	66.67%
	Lum	56.75%.	52.63%	61.11%
	NormGrey	64.86%	68.42 %	61.11%
	NormRGB	67.56%	63.16%	72.22%
	NormRGB-lum	62.16%	68.42%	55.56%

Table 6: Classification results for shoulder/hip region.

Body Part	Color Normalization	Success Rate	Sensitivity	Specificity
Shoulder/Hip With 34 Dogs cancer: 24 non-cancer: 22	Original	61.70%	65.22%	58.33%
	Lum	71.73%	72.73%	70.83%
	NormGrey	67.39%	81.82%	54.17%
	NormRGB	63.04%	72.73%	54.17%
	NormRGB-lum	67.39%	75.00%	59.09%

Table 7: Classification results for wrist region.

Body Part	Color Normalization	Success Rate	Sensitivity	Specificity
Wrist With 34 Dogs cancer: 32 non-cancer: 31	Original	69.84%.	75.00%	64.52%
	Lum	68.25%.	61.29%	75.00%
	NormGrey	68.25%	64.52 %	71.88%
	NormRGB	61.90%	58.06%	65.63%
	NormRGB-lum	68.25%	74.19%	62.50%

Table 8: Best classification results for different body parts.

Body Part	**Color Normalization**	**Success Rate**	**Sensitivity**	**Specificity**
Elbow Knee	Lum	64.92%	61.76%	68.18%
Full Limb	NormRGB	67.56%	63.16%	72.22%
Shoulder/Hip	Lum	71.73%	72.73%	70.83%
Wrist	Original	69.84%.	75.00%	64.52%

All of the above experiments were performed with texture pixel distance of six. Research was carried out concurrently with different pixel distances and it was determined that a pixel distance of seven provides the overall best result for this application. The value of texture distance was thus set to seven for the subsequent research experiments.

The same experiments were performed again with more images from 5 dogs making a total of 39 dogs. The main reason behind running the same experiments with more images was to check if we get a more complete data set with addition of more images. Histogram features, spectral features and texture features with a pixel distance of seven were extracted. Standard normal density and softmax scaling data normalization methods and two pattern classification methods, nearest neighbor and K nearest neighbor with K=5 were used for these experiments and this value was chosen experimentally. All the experiments were performed for original as well as color normalized group. The following tables show the result of experiments for four different body parts with five color normalized group.

Table 9: Classification results for elbow knee region.

Body Part	Color Normalization	Success Rate	Sensitivity	Specificity
Elbow Knee With 39 Dogs cancer: 71 non-cancer: 73	Original	63.88%	57.75%	69.86%
	Lum	66.66%	65.75%	67.61%
	NormGrey	65.97%	67.61%	64.38%
	NormRGB	61.80%	60.56%	63.01%
	NormRGB-lum	63.88%	68.49%	59.15%

For the elbow/knee region the best classification success rate of 66.66% was achieved with lum as color normalization method. However the results from all five sets are reasonably close. The different features used for best classification for different color normalization is shown by table below.

Table 10: Features, data normalization and pattern classification methods used for best classification.

Body Part	Color Normalization	Features	Data Normalization	Pattern Classification
Elbow Knee With 39 Dogs cancer: 71 non-cancer: 73	Original	Histogram Std. Dev Histogram Energy	Standard Normal	KNN5
	Lum	Histogram Mean Histogram Std. dev. Histogram Energy Histogram Entropy	Soft-max, r = 1	KNN5
	NormGrey	Spectral Texture Inertia Texture Correlation Histogram Std. dev. Histogram Skew	Standard Normal	NN
	NormRGB	Texture Energy Histogram Energy Histogram Entropy	Standard Normal	KNN5
	NormRGB-lum	Texture Energy Histogram Skew Histogram Energy Histogram Entropy	None	NN

Table 11: Classification results for full limb region.

Body Part	Color Normalization	Success Rate	Sensitivity	Specificity
Full Limb With 39 Dogs cancer: 26 non-cancer: 26	Original	68.62%	60.00%	76.92%
	Lum	74.50%	72.00%	76.92%
	NormGrey	68.62%	61.54%	76.00%
	NormRGB	76.47%	68.00%	84.62%
	NormRGB-lum	74.50%	68.00%	80.77%

Table 12: Features, data normalization and pattern classification methods used for best classification.

Body Part	Color Normalization	Features	Data Normalization	Pattern Classification
Full Limb With 39 Dogs cancer: 26 non-cancer: 26	Original	Spectral Texture Correlation	Standard Normal	NN
	Lum	Spectral Texture Energy Texture Correlation Histogram Std. Dev. Histogram Skew	Soft-max, r = 1	KNN5
	NormGrey	Histogram Mean Histogram Skew	None	NN
	NormRGB	Texture Correlation Texture Inv. Diff. Histogram Skew Histogram Energy Histogram Entropy	Soft-max, r = 1	NN
	NormRGB-lum	Spectral Histogram Mean Histogram Skew	Standard Normal	NN

Table 13: Classification results for shoulder/hip region.

Body Part	Color Normalization	Success Rate	Sensitivity	Specificity
Shoulder/Hip With 39 Dogs cancer: 28 non-cancer: 26	Original	66.67%	67.86%	65.38%
	Lum	66.67%	64.29%	69.23%
	NormGrey	64.81%	60.71%	69.23%
	NormRGB	61.11%	60.71%	61.54%
	NormRGB-lum	68.51%	75.00%	61.54%

Table 14: Features, data normalization and pattern classification methods used for best classification for shoulder/hip region.

Body Part	Color Normalization	Features	Data Normalization	Pattern Classification
Shoulder/Hip With 39 Dogs cancer: 28 non-cancer: 26	Original	Histogram Energy	Standard Normal	NN
	Lum	Texture Correlation Histogram Std. Dev.	None	NN
	NormGrey	Texture Correlation Histogram Std. Dev.	Soft-max, r = 1	NN
	NormRGB	Histogram Energy	Soft-max, r = 1	NN
	NormRGB-lum	Texture Energy Texture Inertia Texture Correlation Histogram Std. Dev. Histogram Skew	Standard Normal	NN

Table 15: Classification results for wrist region.

Body Part	Color Normalization	Success Rate	Sensitivity	Specificity
Wrist With 39 Dogs cancer: 35 non-cancer: 34	Original	71.01%	71.43%	70.59%
	Lum	73.91%	68.57%%	79.41%
	NormGrey	76.81%	77.14%	76.47%
	NormRGB	66.67%	58.82%	74.29%
	NormRGB-lum	71.01%	68.57%	73.53%

Table 16: Features, data normalization and pattern classification methods used for best classification.

Body Part	Color Normalization	Features	Data Normalization	Pattern Classification
Wrist With 39 Dogs cancer: 35 non-cancer: 34	Original	Texture Correlation Texture Entropy Histogram Energy Histogram Entropy	Soft-max, r = 1	NN
	Lum	Histogram Mean	Soft-max, r = 1	KNN5
	NormGrey	Texture Correlation Texture InvDiff Texture Entropy Histogram Energy	Standard Normal	NN
	NormRGB	Texture Inertia Histogram Mean Histogram Skew	Standard Normal	NN
	NormRGB-lum	Texture Energy Texture InvDiff Texture Entropy Histogram Skew Histogram Energy Histogram Entropy	Soft-max, r = 1	KNN5

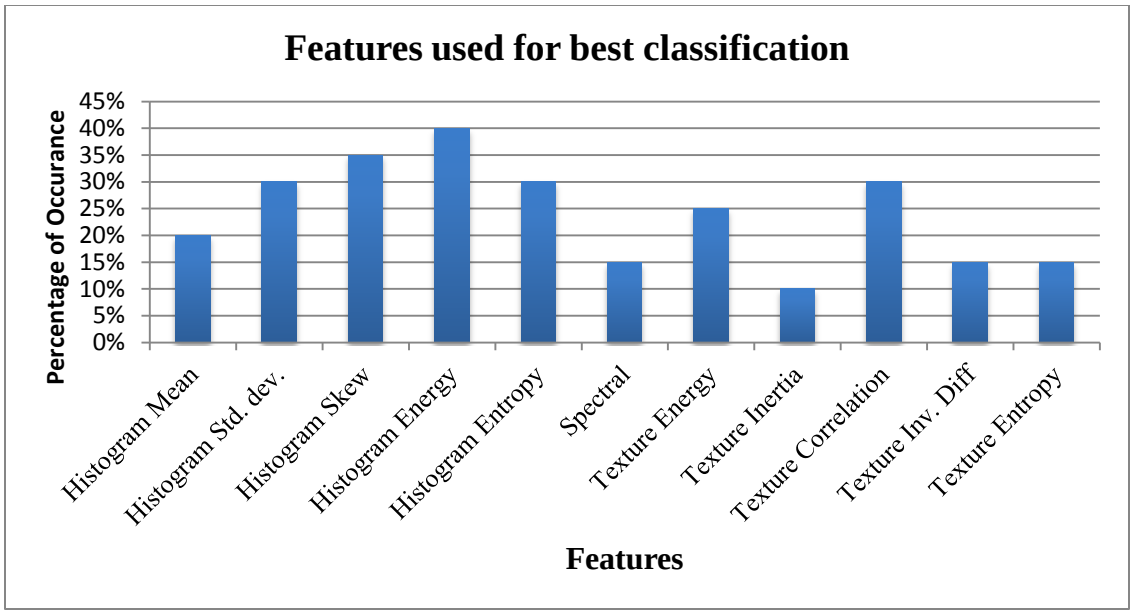

Figure 16: Occurrence of different features for best classification with different body parts for different color normalizations.

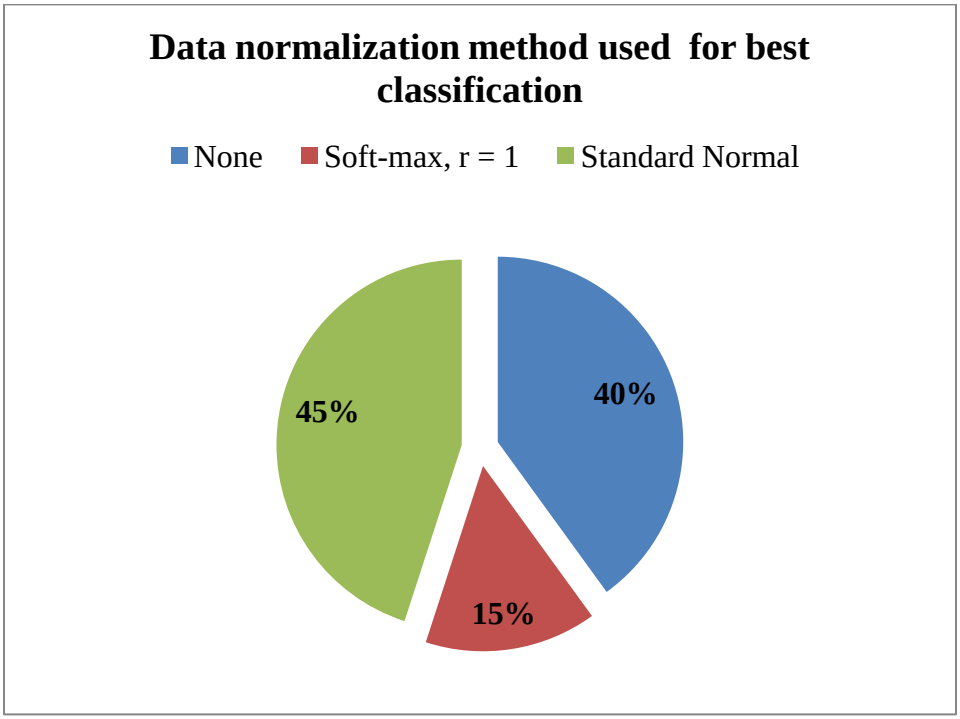

Figure 17: Use of data normalization for best classification with different body parts for different color normalizations.

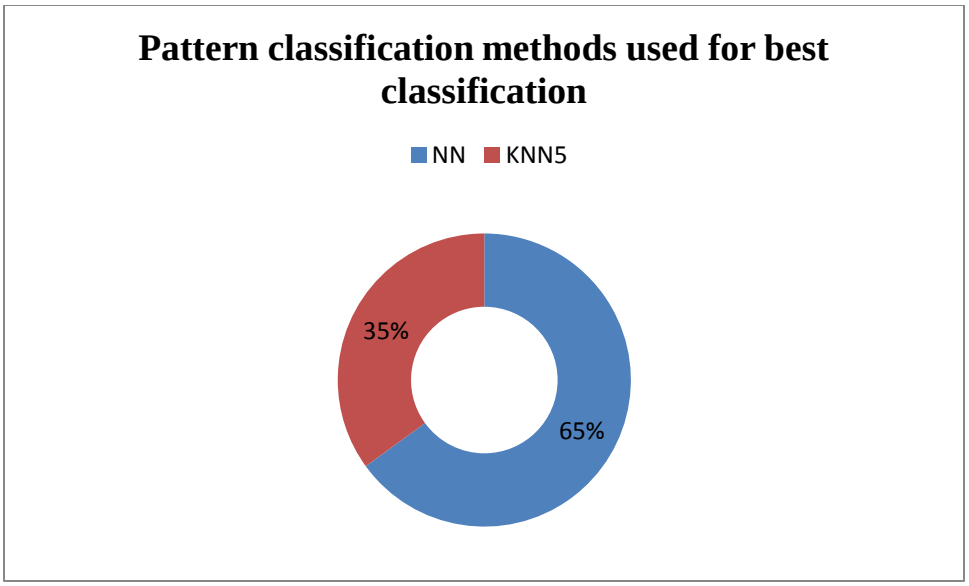

Figure 18: Use of pattern classification algorithms for best classification with different body parts for different color normalizations.

The two figures above show which features and data normalization methods were mostly used for best classification for different experiments with different body parts and color normalizations. Among 20 experiments with different body parts and color normalization, histogram energy was used 40% of the time while texture inertia was least used only 10% of the time. Standard normal and none were used almost equally for data normalization while softmax was used least. For the pattern classification algorithm, nearest neighbor was used 65% time for best classification compared to k-nearest neighbor which was used only 35% of the time.

After running experiments with two data sets, a comparison was made to see if there was any improvement on the results after the addition of images. The comparison table below shows only slight improvement in the results with addition of more samples, however the overall result was not satisfactory.

Table 17: Comparison table showing the best classification results for two different data sets for different body parts.

Body Part	Color Normalization		Success Rate		Sensitivity		Specificity	
	34 Dogs	39 Dogs	34 Dogs	39 Dogs	34 Dogs	39 Dogs	34 Dogs	39 Dogs
Elbow/Knee	lum	lum	64.92%	66.66%	61.76%	65.75%	68.18%	67.61%
Full Limb	Norm RGB	Norm RGB	67.56%	76.47%	63.16%	68.00%	72.22%	80.77%
Shoulder /Hip	lum	Norm RGB-lum	71.73%.	68.51%	72.73%	75.00%	70.83%	61.54%
Wrist	orig	Norm Grey	69.84%	76.81%	75.00%	77.14 %	64.52%	76.47%

The comparison table above shows the overall success rate, sensitivity and specificity after adding more samples to original images. The result shows slight improvement with the addition of more samples which was not significant may be either because sample was complete or the images added were from the same domain of the original images.

This result invokes more questions related to grouping of images. So the images were divided into two group based on the hair type of the dogs namely short hair and long hair to check weather hair might be important factor for separating the images into different groups. The features extracted, data normalization methods and pattern classification methods used were not changed for performing these experiments and were same as previous experiments.

Table 18: Classification result of all limb regions for long hair type animal.

Body Part	Color Normalization	Success Rate	Sensitivity	Specificity
All Limb (39 Dogs) Long Hair cancer: 56 non-cancer: 56	Original	71.42%	71.43%	71.43%
	Lum	66.96%	67.86%	66.07%
	NormGrey	67.85%	76.79%	58.93%
	NormRGB	71.42%	71.43%	71.43%
	NormRGB-lum	69.64%	73.21%	66.07%

Table 19: Classification result of all limb regions for short hair type animal.

Body Part	Color Normalization	Success Rate	Sensitivity	Specificity
All Limb (39 Dogs) Short Hair cancer: 104 non-cancer: 103	Original	67.63%	66.35%	68.93%
	Lum	68.59%	72.12%	65.05%
	NormGrey	63.76%	62.50%	65.05%
	NormRGB	64.73%	66.35%	63.11%
	NormRGB-lum	65.21%	64.08%	66.02%

The result after dividing the images based on the hair types does not show any significant improvement in the result. However a conclusion cannot be made based only on this result about effect of hair on thermographic image analysis as the images from all the limbs, camera view, body parts, gender and breed was not considered. But a conclusion can be made that hair type alone cannot be a factor for image classification. The features, data normalization method and pattern classification method used for best classification for various color normalization methods are shown in tables below.

Table 20: Features, data normalization and pattern classification methods used for best classification.

Body Part	Color Normalization	Features	Data Normalization	Pattern Classification
All Limb (39 Dogs) Long Hair cancer: 56 non-cancer: 56	Original	Texture Correlation Histogram Std. Dev.	Soft-max, r = 1	NN
	Lum	Texture Inertia Texture Correlation Histogram Mean Histogram Std. Dev. Histogram Energy Histogram Entropy	Standard Normal	NN
	NormGrey	Spectral Texture InvDiff Texture Entropy Histogram Mean Histogram Skew Histogram Energy	Standard Normal	KNN5
	NormRGB	Texture Inertia Histogram Energy	Soft-max, r = 1	NN
	NormRGB-lum	Spectral Texture Energy Histogram Mean Histogram Std. Dev. Histogram Skew Histogram Entropy	Standard Normal	KNN5

Table 21: Features, data normalization and pattern classification methods used for best classification.

Body Part	Color Normalization	Features	Data Normalization	Pattern Classification
All Limb (39 Dogs) Short Hair cancer: 104 non-cancer: 103	Original	Texture Energy Texture Entropy Histogram Entropy	Soft-max, r = 1	NN
	Lum	Histogram Mean Histogram Std. Dev.	Standard Normal	KNN5
	NormGrey	Texture Inertia Texture Entropy Histogram Mean Histogram Energy Histogram Entropy	Standard Normal	NN
	NormRGB	Texture Inertia Histogram Skew Histogram Energy	Soft-max, r = 1	NN
	NormRGB-lum	Texture Inertia Texture Correlation Texture Entropy Histogram Mean Histogram Std. Dev. Histogram Skew Histogram Energy Histogram Entropy	Soft-max, r = 1	NN

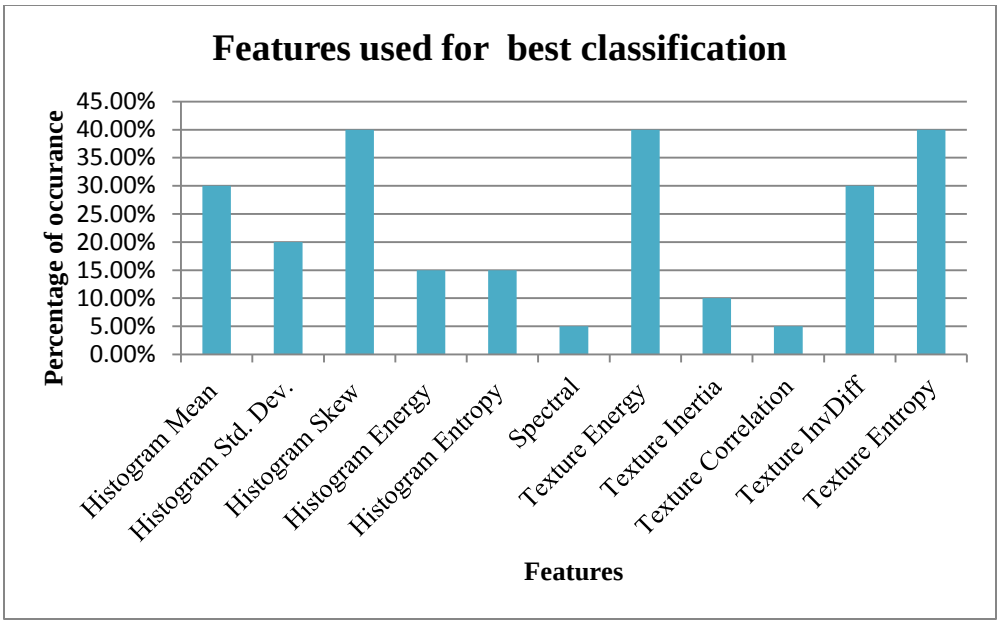

Figure 19: Occurrence of different features for best classification for long and short hair types with different color normalizations.

Figure 19 above shows which features were mostly used for best classification for the experiment with different hair types. It can be seen that histogram features are mostly used for classification, histogram energy being used the most with 70% of the time.

After analyzing the result and discussion with researcher from LIVS, we decided to divide the images into two groups, upper body parts and lower body parts and exclude images that do not fit on either group. Until the end of this stage we were trying to find how thermographic images can be grouped for running experiments to obtain a better result. At the same time results were analyzed to see which features, data normalization methods and pattern classifications techniques were prevailing.

Table 22: Classification result of all limb for upper body parts.

Body Part	Color Normalization	Success Rate	Sensitivity	Specificity
All Limb (39 Dogs) **Upper Body** cancer: 76 non-cancer: 74	Original	73.33%	75.00%	71.62%
	Lum	71.33%	72.37%	70.27%
	NormGrey	72.66%	71.05%	74.32%
	NormRGB	70.66%	71.05%	70.27%
	NormRGB-lum	73.33%	71.05%	75.68%

Table 23: Classification result of all limb for lower body parts.

Body Part	Color Normalization	Success Rate	Sensitivity	Specificity
All Limb (39 Dogs) **Lower Body** cancer: 66 non-cancer: 67	Original	60.10%	57.58%	62.69%
	Lum	60.15%	65.15%	55.22%
	NormGrey	69.92%	71.21%	68.66%
	NormRGB	69.17%	74.24%	64.18%
	NormRGB-lum	64.66%	59.09%	70.15%

The results after dividing images based on the body area, upper and lower body was little better compared to whole limb experiments and hair type experiments, but was lower than the result obtained from different body parts. This result along with previous results show that division of images based on body parts is important factor to be considered. Dividing images considering all these facts could produce better result as the data set will be more homogenous. However due to limited data sets, these experiments were not performed. The tables below show the features, data normalization and pattern classification method that were used for the best classification results.

Table 24: Features, data normalization and pattern classification methods used for best classification.

Body Part	Color Normalization	Features	Data Normalization	Pattern Classification
All Limb (39 Dogs) **Upper Body** cancer: 76 non-cancer: 74	Original	Texture Energy Texture Correlation Histogram Entropy	Soft-max, r = 1	KNN5
	Lum	Texture Correlation Histogram Mean Histogram Entropy	None	NN
	NormGrey	Texture Energy Texture InvDiff Texture Entropy Histogram Std. Dev.	Soft-max, r = 1	KNN5
	NormRGB	Texture Energy Texture Entropy Histogram Std. Dev.	Soft-max, r = 1	KNN5
	NormRGB-lum	Texture Energy Texture Inertia Histogram Mean Histogram Std. Dev. Histogram Skew Histogram Energy	Soft-max, r = 1	KNN5

Table 25: Features, data normalization and pattern classification methods used for best classification.

Body Part	Color Normalization	Features	Data Normalization	Pattern Classification
All Limb (39 Dogs) **Lower Body** cancer: 66 non-cancer: 67	Original	Spectral	Soft-max, r = 1	NN
	Lum	Texture Energy Texture InvDiff Histogram Skew	Soft-max, r = 1	NN
	NormGrey	Texture Correlation Histogram Mean Histogram Std. Dev. Histogram Skew Histogram Energy	Standard Normal	KNN5

	NormRGB	Texture Entropy Histogram Mean Histogram Std. Dev. Histogram Energy	Standard Normal	KNN5
	NormRGB-lum	Texture Inertia Histogram Std. Dev.	Soft-max, r = 1	NN

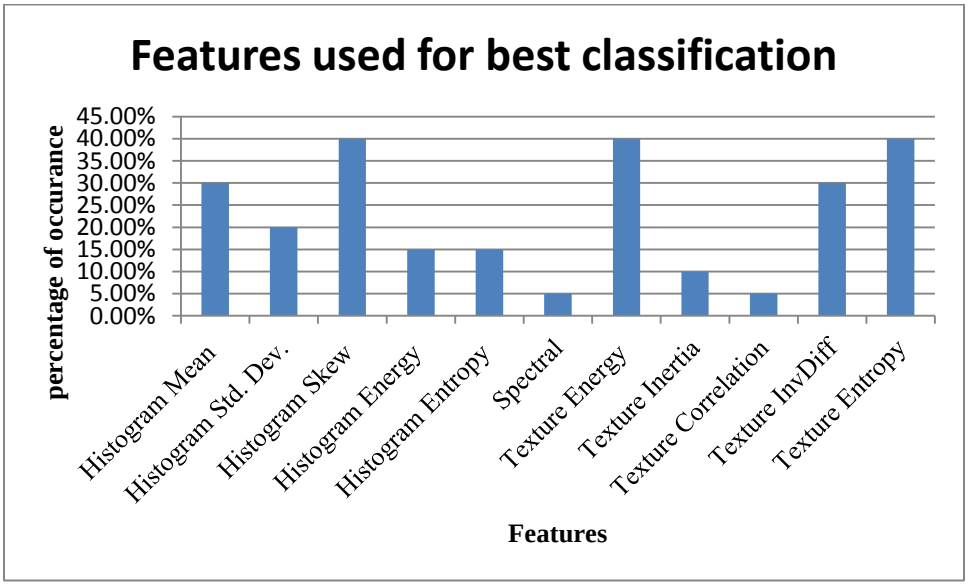

Figure 20: Occurrence of different features for best classification for upper and lower body with different color normalizations.

Figure 20 shows histogram skew and texture energy as most useful features for classifying images. It has been found that there is no fixed trend of features that were used for classifications. However, features such as texture energy and histogram features are prevailing in the best experiments.

The next division was based on limb classification. For the same dogs, hind limbs and forelimbs are different by nature. So it seems logical to divide images based on fore and hind limbs. Thus the images were first divided into two groups based on limbs, forelimb and hindlimb. After that they were divided into two groups based on camera views, anterior and lateral. Color normalization was then performed to each of the subgroups and experiments

were conducted using CVIP-FEPC. Ten features for original images and eleven features for color normalized groups were extracted. Two data normalization method and two pattern classification methods were used for pattern classification. The tables below show the best classification success rate along with sensitivity and specificity for all the experimental sets.

Table 26: Classification success rate for Forelimb for different camera view

Limb	Camera View	Color Normalization	Success Rate	Sensitivity	Specificity
Fore Limb	Anterior	Original	69.56%	91.67%	45.45%
		Lum	69.56%	66.67%	72.73%
		NormGrey	82.60%	91.67%	72.73%
		NormRGB	73.91%	58.33%	90.91%
		NormRGB-lum	82.60%	91.67%	72.73%
	Lateral	Original	62.96%	71.43%	53.85%
		Lum	66.67%	42.86%	92.31%
		NormGrey	74.07%	78.57%	69.23%
		NormRGB	59.25%	57.14%	61.54%
		NormRGB-lum	74.07%	57.14%	61.54%

Table 27: Classification success rate for Hindlimb for different camera view

Limb	Camera View	Color Normalization	Success Rate	Sensitivity	Specificity
Hind Limb	Anterior	Original	90.90%	81.82%	100.00%
		Lum	86.36%	81.82%	90.91%
		NormGrey	90.90%	90.91%	90.91%
		NormRGB	77.27%	72.73%	81.82%
		NormRGB-lum	77.27%	72.73%	81.82%
	Lateral	Original	77.27%	81.82%	72.73%
		Lum	77.27%	90.91%	63.64%
		NormGrey	81.82%	72.73%	90.91%
		NormRGB	77.27%	90.91%	63.64%
		NormRGB-lum	77.27%	100.00%	54.55%

The table above shows that a much better result was achieved from the experiments after dividing images based on front and hind limb and camera view. A success rate of 82.60% with sensitivity of 91.67% and specificity of 72.73% was achieved for fore limb with anterior view. In the similar manner success rate of 90.90% with sensitivity of 90.91% and specificity of 90.91% was achieved for hind limb with anterior view. The overall success rate, sensitivity and specificity for experiments with all views and color normalizations were better than the results obtained so far. This indicates the importance of separating images based on camera view as well.

Table 28: Features, data normalization and pattern classification methods used for best classification.

Limb	Camera View	Color Normalization	Features	Data Normalization	Pattern Classification
Fore Limb	Anterior	Original	Texture Entropy	Soft-max, r = 1	NN
		Lum	Texture Entropy Histogram Mean	Soft-max, r = 1	NN
		NormGrey	Texture InvDiff Histogram Skew	Soft-max, r = 1	NN
		NormRGB	Texture Energy Texture InvDiff Histogram Skew	Standard Normal	KNN5
		NormRGB-lum	Histogram Mean Histogram Skew	Soft-max, r = 1	NN
	Lateral	Original	Texture Correlation Histogram StdDev Histogram Energy Histogram Entropy	Standard Normal	NN
		Lum	Texture Energy Histogram Mean Histogram Skew	Standard Normal	KNN5
		NormGrey	Texture Entropy Histogram Skew	Soft-max, r = 1	NN
		NormRGB	Texture Inertia Histogram Skew	Standard Normal	NN
		NormRGB-lum	Texture Entropy Histogram Mean Histogram Skew	Soft-max, r = 1	NN

Table 29: Features, data normalization and pattern classification methods used for best classification.

Limb	Camera View	Color Normalization	Features	Data Normalization	Pattern Classification
Hind Limb	Anterior	Original	Texture Entropy Histogram Skew	Soft-max, r = 1	KNN5
		Lum	Texture Energy Histogram Mean Histogram StdDev Histogram Skew	Soft-max, r = 1	NN
		NormGrey	Texture Energy Texture InvDiff Histogram Mean	Standard Normal	NN
		NormRGB	Texture Inertia Texture InvDiff Texture Entropy Histogram Mean Histogram Entropy	Soft-max, r = 1	NN
		NormRGB-lum	Texture Energy Texture Entropy	Soft-max, r = 1	KNN5
	Lateral	Original	Spectral Texture Energy Texture InvDiff Texture Entropy Histogram StdDev Histogram Skew Histogram Energy	Standard Normal	NN
		Lum	Texture Entropy	None	KNN5
		NormGrey	Histogram StdDev	None	NN
		NormRGB	Texture Energy Texture Inertia Texture InvDiff Histogram Energy	Soft-max, r = 1	NN
		NormRGB-lum	Texture Energy	None	KNN5

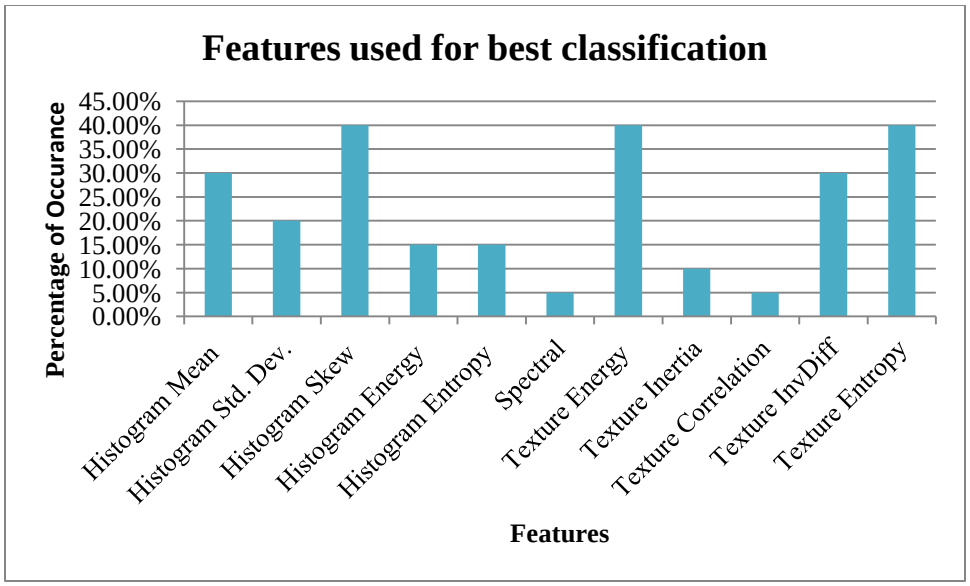

Figure 21: Occurrence of different features for best classification for forelimb and hindlimb with different camera views and color normalizations.

The features that were used for best classification are shown in figure 21. Histogram skew and texture energy and entropy were again the most used features for best classification. Spectral features were the least used features as in previous experiments.

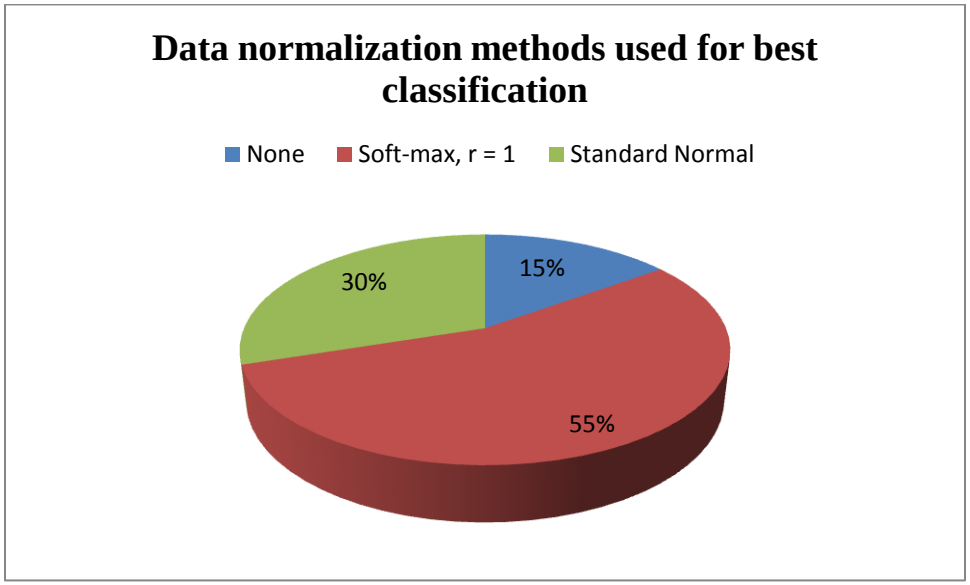

Figure 22: Data normalization methods used for best classification for forelimb and hindlimb with different camera views and color normalizations.

Softmax scaling was the most used with 55% of the time followed by standard normal with 30% and none with 15%. Nearest neighbor was mostly used for pattern classification with 70% of the time.

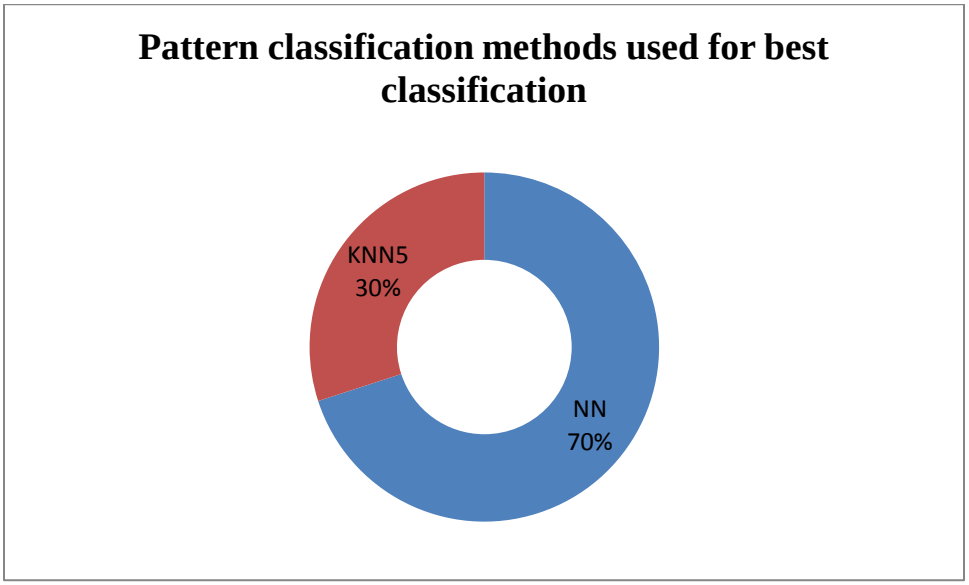

Figure 23: Pattern classification methods used for best classification for forelimb and hindlimb with different camera views and color normalizations.

5.3 Third Stage of Experiment

After analyzing the results from the first stage and second stage of the experiments, we conclude that the homogeneity in data set is an important factor for classification. So dividing samples into different sets based on body parts, camera view, body area, types of limb, gender and breed is necessary. However, due to limited sample sets the division based on all these factors was not possible. However, we decided to divide the images based on body parts and camera views. This was because a better result was obtained after dividing images into front and hind limbs along with camera views. There were 161 cancerous images and 161 non cancerous images from 41 dogs. The images were first divided into four groups according to body parts (Elbow Knee, Full Limb, Shoulder/Hip and Wrist). Each of the groups were then further divided into four groups according to views (Anterior, Lateral, Medial and Posterior). However, experiments with small data sets were not considered (shown by red color in following table)

Table 30: Division of images into different subgroups for experiment

Body Part	Anterior	Lateral	Medial	Posterior
Elbow Knee	Cancer = 20 No cancer= 21	Cancer = 29 No cancer= 31	Cancer = 5 No cancer=4	Cancer = 17 No cancer=17
Full Limb	Cancer = 5 No cancer=5	Cancer = 16 No cancer=17	Cancer = 2 No cancer=2	Cancer = 2 No cancer=2
Shoulder Hip	Cancer = 3 No cancer=2	Cancer = 20 No cancer=20	Cancer = 2 No cancer=2	Cancer = 3 No cancer=1
Wrist	Cancer = 12 No cancer=11	Cancer = 15 No cancer=14	Cancer = 3 No cancer=3	Cancer = 7 No cancer=8

Four color normalization methods were then applied to each subgroup, so including the original images; this makes forty five experimental sets. Ten features, two data normalization techniques and two pattern classification methods were used for each experimental set which results in total of 82,944 individual experiments. These individual experiments were then analyzed to find which camera view and color normalization method

gave best classification success. Two important metrics, sensitivity and specificity, were also measured for the experiment that provides the best classification success.

Table 31: Classification success rate for Elbow/Knee for different camera view

Body Part	Camera View	Color Normalization	Success Rate	Sensitivity	Specificity
Elbow Knee	Anterior	Original	73.17%	70.00%	76.19%
		Lum	75.60%	80.00%	71.43%
		NormGrey	82.92%	85.00%	80.95%
		NormRGB	87.80%	80.00%	95.24%
		NormRGB-lum	80.48%	80.00%	80.95%
	Lateral	Original	60.00%	58.62%	61.29%
		Lum	68.33%	68.97%	67.74%
		NormGrey	68.33%	68.97%	67.74%
		NormRGB	63.33%	58.62%	67.74%
		NormRGB-lum	65.00%	68.29%	61.29%
	Posterior	Original	76.47%	70.59%	82.35%
		Lum	73.52%	58.42%	88.24%
		NormGrey	76.47%	58.82%	94.12%
		NormRGB	76.47%	82.35%	70.59%
		NormRGB-lum	76.47%	64.71%	88.24%

Table 32: Features, data normalization and pattern classification methods used for best classification for elbow/knee region.

Body Part	Camera View	Color Normalization	Features	Data Normalization	Pattern Classification
Elbow/ Knee	Anterior	Original	Texture Energy Texture Inv Diff	None	NN
		Lum	Texture Energy Texture Correlation Texture InvDiff Texture Entropy Histogram Mean Histogram StdDev Histogram Skew Histogram Energy Histogram Entropy	Soft-max, r = l	NN
		NormGrey	Texture Inertia Texture InvDiff Histogram Skew	Soft-max, r = l	KNN5
		NormRGB	Texture Inertia Texture Entropy Histogram Mean Histogram Stddev Histogram Skew Histogram Energy Histogram Entropy	Soft-max, r = l	NN
		NormRGB-lum	Spectral Texture Inertia Histogram Mean Histogram Stddev Histogram Skew Histogram Energy	Soft-max, r = l	KNN5
	Lateral	Original	Histogram Std Dev	Soft-max, r = l	NN
		Lum	Histogram Mean Histogram StdDev Histogram Energy Histogram Entropy	Soft-max, r = l	NN

		NormGrey	Texture Inertia Texture Entropy Histogram Mean Histogram Skew	Soft-max, r = l	KNN5
		NormRGB	Texture Entropy Histogram Skew	Soft-max, r = l	KNN5
		NormRGB-lum	Histogram Skew	None	NN
	Posterior	Original	Histogram StdDev Histogram Energy	Standard Normal	KNN5
		Lum	Texture InvDiff Histogram Mean	Soft-max, r = l	KNN5
		NormGrey	Histogram Mean Histogram Skew	Soft-max, r = l	KNN5
		NormRGB	Texture Inertia Histogram Std Dev	None	NN
		NormRGB-lum	Histogram Mean Histogram StdDev Histogram Skew	Soft-max, r = l	KNN5

Table 33: Classification success rate for Full limb region for different camera view

Body Part	Camera View	Color Normalization	Success Rate	Sensitivity	Specificity
Full Limb	Anterior	Original	70.00%	100.00%	40.00%
		Lum	70.00%	80.00%	60.00%
		NormGrey	80.00%	80.00%	80.00%
		NormRGB	80.00%	80.00%	80.00%
		NormRGB-lum	90.00%	100.00%	80.00%
	Lateral	Original	72.72%	68.75%	76.47%
		Lum	72.72%	68.75%	76.47%
		NormGrey	84.84%	81.25%	88.24%
		NormRGB	75.75%	81.25%	70.59%
		NormRGB-lum	78.78%	87.50%	70,59%

Table 34: Features, data normalization and pattern classification methods used for best classification for full limb region.

Body Part	Camera View	Color Normalization	Features	Data Normalization	Pattern Classification
Full Limb	Anterior	Original	Texture correlation Histogram Energy	None	NN
		Lum	Histogram Energy	Soft-max, r = l	NN
		NormGrey	Spectral	Soft-max, r = l	NN
		NormRGB	Spectral	Standard Normal	NN
		NormRGB-lum	Histogram Mean Histogram Std Dev	None	NN
	Lateral	Original	Texture Correlation	Soft-max, r = l	NN
		Lum	Texture Correlation	Soft-max, r = l	NN
		NormGrey	Texture InvDiff Histogram StdDev Histogram Skew Histogram Entropy	Soft-max, r = l	NN
		NormRGB	Texture Energy Texture Inertia Histogram Skew Histogram Entropy	Soft-max, r = l	NN
		NormRGB-lum	Texture Inertia Texture InvDiff Texture Entropy Histogram StdDev Histogram Skew Histogram Energy Histogram Entropy	Soft-max, r = l	NN

Table 35: Classification success rate for Shoulder/Hip for different camera view

Body Part	Camera View	Color Normalization	Success Rate	Sensitivity	Specificity
Shoulder/Hip	Lateral	Original	65.00%	50.00%	80.00%
		Lum	72.50%	80.00%	65.00%
		NormGrey	62.50%	70.00%	55.00%
		NormRGB	67.50%	60.00%	75.00%
		NormRGB-lum	75.00%	70.00%	80.00%

Table 36: Features, data normalization and pattern classification methods used for best classification for shoulder/hip region.

Body Part	Camera View	Color Normalization	Features	Data Normalization	Pattern Classification
Shoulder/Hip	Lateral	Original	Texture Inertia Texture InvDiff Histogram StdDev Histogram Skew Histogram Energy Histogram Entropy	Standard Normal	KNN5
		Lum	Texture Inertia Histogram Skew	Soft-max, r = l	KNN5
		NormGrey	Texture InvDiff Texture Entropy	Soft-max, r = l	KNN5
		NormRGB	Texture Entropy Histogram Skew Histogram Entropy	None	NN
		NormRGB-lum	Texture Correlation Histogram Skew	Soft-max, r = l	NN

Table 37: Classification success rate for Wrist for different camera view

Body Part	Camera View	Color Normalization	Success Rate	Sensitivity	Specificity
Wrist	Anterior	Original	73.91%	75.00%	72.73%
		Lum	82.60%	91.67%	72.73%
		NormGrey	78.26%	83.33%	72.73%
		NormRGB	73.91%	83.33%	63.64%
		NormRGB-lum	73.91%	83.33%	63.64%
	Lateral	Original	79.31%	86.67%	71.43%
		Lum	79.31%	93.33%	64.29%
		NormGrey	75.86%	80.00%	71.43%
		NormRGB	79.31%	80.00%	78.57%
		NormRGB-lum	89.65%	86.67%	92.86%
	Posterior	Original	93.33%	100.00%	87.00%
		Lum	93.33%	100.00%	87.50%
		NormGrey	73.33%	85.71%	62.50%
		NormRGB	93.33%	100.00%	87.50%
		NormRGB-lum	100.00%	100.00%	100.00%

Table 38 : Features, data normalization and pattern classification methods used for best classification for wrist region.

Body Part	Camera View	Color Normalization	Features	Data Normalization	Pattern Classification
Wrist	Anterior	Original	Texture InvDiff Histogram Energy	None	NN
		Lum	Texture Energy Texture Entropy Histogram Mean	Soft-max, r = l	NN
		NormGrey	Texture Correlation Texture Entropy Histogram Skew	Standard Normal	NN
		NormRGB	Texture Inertia	None	NN
		NormRGB-lum	Texture Entropy Histogram Mean Histogram Entropy	Soft-max, r = l	NN
	Lateral	Original	Texture Correlation Texture InvDiff Texture Entropy Histogram Entropy	Soft-max, r = l	KNN5
		Lum	Texture Entropy Histogram Mean	Standard Normal	KNN5
		NormGrey	Texture Energy Texture Inertia Texture Entropy	Soft-max, r = l	NN
		NormRGB	Texture Correlation Texture Entropy	Standard Normal	NN
		NormRGB-lum	Histogram Mean	None	NN
	Posterior	Original	Texture Inertia Texture Correlation Texture InvDiff Texture Entropy	Soft-max, r = l	NN
		Lum	Texture Correlation Histogram Entropy	None	NN
		NormGrey	Spectral	None	NN
		NormRGB	Texture Energy	Soft-max, r = l	NN
		NormRGB-lum	Texture Energy Texture Inertia Histogram Entropy	Standard Normal	NN

Table 39: Best classification results for different body parts.

Body Part	Camera View	Color Normalization	Success Rate	Sensitivity	Specificity
Elbow Knee	Anterior	normRGB	87.80%	80.00%	95.20%
Full Limb	Anterior	normRGB-lum	90.00%	100.00%	80.00%
Shoulder/Hip	Lateral	normRGB-lum	75.00%	70.00%	80.00%
Wrist	Lateral	normRGB-lum	89.65%	86.67%	92.86%

The table shows that, for example Elbow/Knee Anterior view, 87.8% overall success with sensitivity 80% and specificity 95.2% was achieved with normRGB color normalization. These results show that the NormRGB and NormRGB-lum color normalization methods provided the best results for this application. The best view is dependent on the body part, with the anterior view providing the best results for elbow/knee and full limb, and the lateral view had the best result for shoulder/hip and wrist image sets.

We analyzed the results that provide the best result from all the experimental sets to see which features, data normalization methods and pattern classification methods were mostly used. The purpose of this is to find which features, data normalization methods and pattern classification techniques were most often used for best classification results.

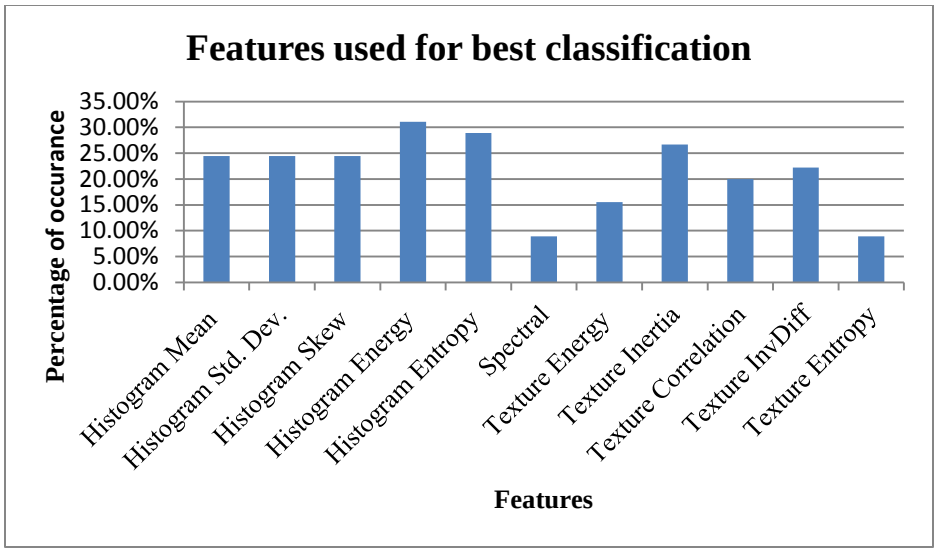

Figure 24: Occurrence of different features for best classification for different body parts with different camera views and color normalizations.

It was determined that histogram features were important for pattern classification. However, a standard pattern of features that were most important was not determined here. There were specific set of features, data normalization and pattern classification methods for individual experimental setup. An algorithm that fits to all experiment was not possible to determine, however best algorithm for a particular type of experimental setup was found. This calls for more experiments with more samples that can be divided based on various factors.

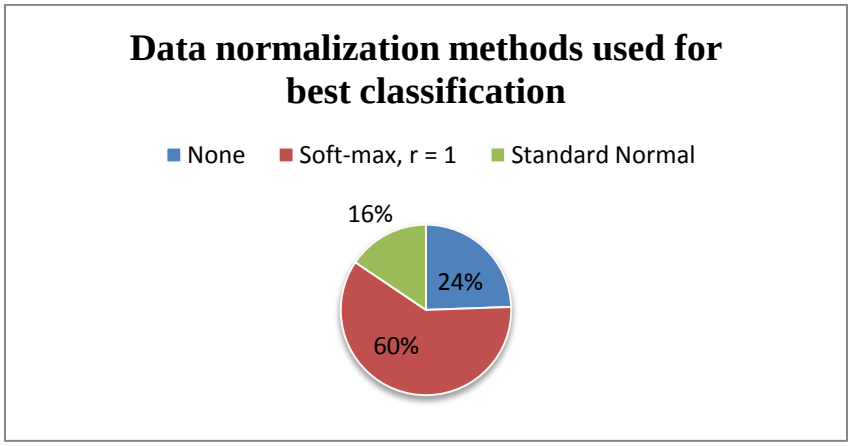

Figure 25: Data normalization methods used for best classification for separate body parts with different camera views and color normalizations.

The above figure shows that softmax scaling as important data normalization method for this application which was used 60% of the time. The figure below shows nearest neighbor as prevailing pattern classification methods with total occurrence of 69%.

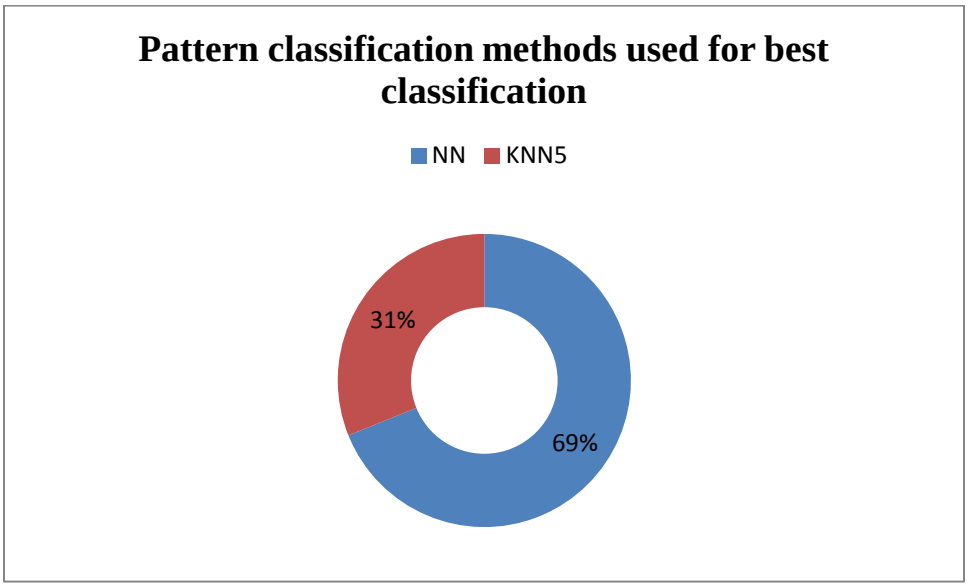

Figure 26: Pattern classification methods used for best classification for separate body parts with different camera views and color normalizations..

There were multiple results with different features, data normalization methods and pattern classification methods that generate the same best result for a particular experimental setup. However, for this research study only those that use few features for pattern classification were considered for analysis. So the figures that show which features, data normalization methods and pattern classification methods were primarily used may not be sufficient. However, they provide a general outline that is important for further investigation on similar studies and also open more areas for further research.

5.4 Fourth Stage of Experiment

At this point we decided to continue with the division that was done on the third stage and perform experiments with other pattern classification tools. The other tools used were the Partek Discovery Suite and Artificial Neural Network.

At first the Partek Discovery Suite was used for pattern classification. Experiments that produce the best result in CVIP-FEPC for each data normalization method were considered for using with Partek. Only those features that were present for best classification on those particular experiments in CVIP_FEPC were used in Partek for pattern classification. Nearest neighbor, K nearest neighbor with k=3 and 5, linear discriminant analysis with equal prior probability, linear discriminant analysis with proportional prior probability, quadratic discriminant analysis with equal prior probability and quadratic discriminant analysis with proportional prior probability were used as pattern classification methods.

Three results each from separate data normalization methods were considered for one experimental set. The reason behind this was because the way pattern classification is done using a data normalized set in CVIP-FEPC is different than Partek Discovery for leave one out experiments. CVIP-FEPC does data normalization separately for the training set and test set. That means the entire data set is normalized before testing and then used as the test set. Separate data normalization is performed for all possible combinations of images and is considered as training set. The leave one out pattern classification is then performed. Since this algorithm is not available in Partek Discovery suite, we choose the feature files where data normalization was done as a whole.

The results for different body parts with various camera views for different color normalization with various data normalization methods are shown by following tables.

Table 40: Classification success rate for Elbow/Knee for anterior view with Partek.

Body Part/ Camera View	Color Normalization	Data Normalization	Success Rate	Sensitivity	Specificity	Pattern Classification
Elbow/Knee Anterior	orig	None	73.17%	70.00%	76.19%	NN
		Soft-max, r = l	73.17%	65.00%	80.95%	NN
		Standard Normal	73.17%	70.00%	76.19%	KNN5
	lum	None	73.17%	70.00%	76.19%	NN
		Soft-max, r = l	75.60%	80.00%	71.42%	NN
		Standard Normal	73.17%	70.00%	76.19%	NN
	normGrey	None	82.92%	90.00%	76.19%	QDAEPP
		Soft-max, r = l	82.92%	85.00%	80.95%	KNN5
		Standard Normal	78.04%	75.00%	80.95%	NN
	normRGB	None	78.04%	80.00%	76.19%	KNN5
		Soft-max, r = l	85.36%	80.00%	90.47%	NN
		Standard Normal	85.36%	85.00%	85.71%	NN
	normRGB-lum	None	70.73%	70.00%	62.50%	KNN3
		Soft-max, r = l	78.04%	75.00%	80.95%	KNN5
		Standard Normal	78.04%	70.00%	85.71%	KNN5

Table 41: Classification success rate for Elbow/Knee for lateral view with Partek.

Body Part/ Camera View	Color Normalization	Data Normalization	Success Rate	Sensitivity	Specificity	Pattern Classification
Elbow/Knee Lateral	orig	None	53.33%	48.27%	58.06%	NN
		Soft-max, r = l	58.33%	58.62%	58.06%	NN
		Standard Normal	53.33%	55.17%	61.29%	NN
	lum	None	60.00%	55.17%	64.51%	NN
		Soft-max, r = l	68.33%	68.96%	67.74%	NN
		Standard Normal	68.33%	68.96%	67.74%	NN
	normGrey	None	66.66%	62.06%	70.96%	KNN5
		Soft-max, r = l	68.33%	58.62%	77.41%	KNN5
		Standard Normal	68.33%	58.62%	77.41%	KNN5
	normRGB	None	60.00%	55.17%	64.51%	KNN5
		Soft-max, r = l	63.33%	58.62%	67.74%	KNN5
		Standard Normal	65.00%	62.06%	67.74%	LDAEPP
	normRGB-lum	None	65.00%	68.29%	61.29%	NN
		Soft-max, r = l	65.00%	68.96%	61.29%	NN
		Standard Normal	65.00%	68.96%	61.29%	NN

Table 42: Classification success rate for Elbow/Knee for Posterior view with Partek.

Body Part/ Camera View	Color Normalization	Data Normalization	Success Rate	Sensitivity	Specificity	Pattern Classification
Elbow/Knee Posterior	orig	None	73.52%	8.23%	58.82%	QDAEPP
		Soft-max, r = l	73.52%	64.70%	82.35%	KNN5
		Standard Normal	76.47%	70.58%	82.35%	KNN5
	lum	None	67.64%	64.70%	70.58%	NN
		Soft-max, r = l	73.52%	58.82%	88.23%	KNN5
		Standard Normal	70.58%	64.70%	76.47%	KNN5
	normGrey	None	64.70%	52.94%	76.47%	NN
		Soft-max, r = l	76.47%	58.82%	94.12%	KNN5
		Standard Normal	73.52%	52.94%	94.12%	KNN5
	normRGB	None	76.47%	82.35%	70.59%	NN
		Soft-max, r = l	67.64%	70.58%	64.70%	NN
		Standard Normal	70.58%	76.47%	64.70%	KNN3
	normRGB-lum	None	70.58%	58.82%	70.58%	LDAEPP
		Soft-max, r = l	76.47%	64.70%	88.23%	KNN5
		Standard Normal	73.52%	76.47%	70.58%	NN

Table 43: Classification success rate for full limb for anterior view with Partek.

Body Part/ Camera View	Color Normalization	Data Normalization	Success Rate	Sensitivity	Specificity	Pattern Classification
Full Limb Anterior	orig	None	70.00%	100.00%	40.00%	NN
		Soft-max, r = l	60.00%	60.00%	60.00%	NN
		Standard Normal	90.00%	80.00%	100.00%	QDAEPP
	lum	None	60.00%	80.00%	40.00%	NN
		Soft-max, r = l	70.00%	80.00%	60.00%	NN
		Standard Normal	70.00%	100.00%	40.00%	LDAEPP
	normGrey	None	70.00%	60.00%	80.00%	NN
		Soft-max, r = l	80.00%	80.00%	80.00%	NN
		Standard Normal	90.00%	80.00%	100.00%	NN
	normRGB	None	90.00%	80.00%	100.00%	QDAEPP
		Soft-max, r = l	60.00%	60.00%	60.00%	NN
		Standard Normal	70.00%	60.00%	100.00%	KNN5
	normRGB-lum	None	90.00%	100.00%	80.00%	NN
		Soft-max, r = l	90.00%	100.00%	80.00%	LDEAPP
		Standard Normal	80.00%	100.00%	60.00%	NN

Table 44: Classification success rate for Full Limb for lateral view with Partek.

Body Part/ Camera View	Color Normalization	Data Normalization	Success Rate	Sensitivity	Specificity	Pattern Classification
Full Limb Lateral	orig	None	69.69%	56.25%	82.35%	NN
		Soft-max, r = l	72.73%	68.75%	76.47%	NN
		Standard Normal	69.69%	56.25%	82.35%	NN
	lum	None	69.69%	56.25%	82.35%	NN
		Soft-max, r = l	72.73%	68.75%	76.47%	NN
		Standard Normal	69.69%	56.25%	82.35%	NN
	normGrey	None	69.69%	62.50%	76.47%	NN
		Soft-max, r = l	84.84%	81.25%	88.23%	NN
		Standard Normal	81.81%	81.25%	82.35%	NN
	normRGB	None	72.72%	57.50%	58.82%	KNN5
		Soft-max, r = l	75.75%	81.25%	70.58%	NN
		Standard Normal	75.75%	93.75%	58.82%	KNN5
	normRGB-lum	None	72.72%	87.50%	58.82%	KNN5
		Soft-max, r = l	75.75%	81.25%	70.58%	NN
		Standard Normal	72.72%	81.25%	64.70%	NN

Table 45: Classification success rate for Shoulder/Hip for lateral view with Partek.

Body Part/ Camera View	Color Normalization	Data Normalization	Success Rate	Sensitivity	Specificity	Pattern Classification
Shoulder/Hip Lateral	orig	None	62.50%	50.00%	75.00%	NN
		Soft-max, r = l	67.50%	65.00%	70.00%	LDAEPP
		Standard Normal	60.00%	45.00%	75.00%	KNN5
	lum	None	67.50%	70.00%	65.00%	NN
		Soft-max, r = l	70.00%	75.00%	65.00%	KNN5
		Standard Normal	65.00%	60.00%	70.00%	NN
	normGrey	None	57.50%	75.00%	40.00%	NN
		Soft-max, r = l	65.00%	65.00%	65.00%	QDAEPP
		Standard Normal	57.00%	66.67%	75.00%	KNN5
	normRGB	None	67.50%	60.00%	75.00%	NN
		Soft-max, r = l	65.00%	55.00%	75.00%	NN
		Standard Normal	62.50%	55.00%	70.00%	NN
	normRGB-lum	None	57.50%	45.00%	70.00%	NN
		Soft-max, r = l	75.00%	70.00%	80.00%	NN
		Standard Normal	62.50%	55.00%	70.00%	NN

Table 46: Classification success rate for Wrist for anterior view with Partek.

Body Part/ Camera View	Color Normalization	Data Normalization	Success Rate	Sensitivity	Specificity	Pattern Classification
Wrist Anterior	orig	None	73.91%	75.00%	72.73%	NN
		Soft-max, r = l	69.56%	81.81%	63.63%	KNN5
		Standard Normal	69.56%	75.00%	63.63%	NN
	lum	None	73.91%	83.33%	63.63%	NN
		Soft-max, r = l	82.60%	91.66%	72.73%	NN
		Standard Normal	82.60%	91.66%	72.73%	NN
	normGrey	None	69.56%	58.33%	81.81%	NN
		Soft-max, r = l	69.56%	66.66%	72.73%	NN
		Standard Normal	73.91%	83.33%	63.63%	NN
	normRGB	None	73.91%	83.33%	63.33%	NN
		Soft-max, r = l	69.56%	75.00%	63.63%	NN
		Standard Normal	73.91%	83.33%	63.33%	NN
	normRGB-lum	None	60.86%	66.66%	54.54%	NN
		Soft-max, r = l	73.91%	83.33%	63.63%	NN
		Standard Normal	78.26%	75.00%	81.81%	NN

Table 47: Classification success rate for Wrist for lateral view with Partek.

Body Part/ Camera View	Color Normalization	Data Normalization	Success Rate	Sensitivity	Specificity	Pattern Classification
Wrist Lateral	orig	None	75.86%	80.00%	71.42%	NN
		Soft-max, r = l	75.86%	80.00%	71.42%	KNN5
		Standard Normal	75.86%	80.00%	71.42%	KNN5
	lum	None	71.42%	80.00%	64.28%	NN
		Soft-max, r = l	75.86%	80.00%	71.42%	NN
		Standard Normal	79.31%	93.33%	64.28%	KNN5
	normGrey	None	72.41%	80.00%	64.28%	NN
		Soft-max, r = l	72.41%	73.33%	71.42%	NN
		Standard Normal	75.86%	73.33%	78.57%	NN
	normRGB	None	72.41%	80.00%	64.28%	KNN5
		Soft-max, r = l	79.31%	80.00%	78.57%	NN
		Standard Normal	75.86%	80.00%	71.42%	NN
	normRGB-lum	None	89.65%	86.67%	92.85%	NN
		Soft-max, r = l	89.65%	86.67%	92.85%	NN
		Standard Normal	89.65%	86.67%	92.85%	NN

Table 48: Classification success rate for Wrist for posterior view with Partek.

Body Part/ Camera View	Color Normalization	Data Normalization	Success Rate	Sensitivity	Specificity	Pattern Classification
Wrist Posterior	orig	None	86.67%	85.71%	87.50%	NN
		Soft-max, r = l	93.33%	100.00%	87.50%	NN
		Standard Normal	93.33%	100.00%	87.50%	NN
	lum	None	93.33%	100.00%	87.50%	NN
		Soft-max, r = l	93.33%	100.00%	87.50%	NN
		Standard Normal	93.33%	100.00%	87.50%	NN
	normGrey	None	73.33%	85.71%	62.50%	NN
		Soft-max, r = l	80.00%	85.71%	75.00%	LDAEPP
		Standard Normal	86.67%	85.71%	87.50%	LDAEPP
	normRGB	None	80.00%	85.71%	75.00%	NN
		Soft-max, r = l	93.33%	100.00%	87.50%	NN
		Standard Normal	93.33%	100.00%	87.50%	NN
	normRGB-lum	None	86.67%	85.71%	87.50%	NN
		Soft-max, r = l	93.33%	85.71%	100.00%	NN
		Standard Normal	93.33%	100.00%	87.50%	NN

Table 49: Best classification results for different body parts with Partek.

Body Part	Camera View	Color Normalization	Data Normalization	Success Rate	Sensitivity	Specificity	Pattern Classification
Elbow/ Knee	Anterior	normRGB	Standard Normal	85.36%	85.00%	85.71%	NN
Full Limb	Anterior	normRGB-lum	none	90.00%	100.00%	80.00%	NN
Shoulder /Hip	Lateral	normRGB-lum	Soft-max, r = l	75.00%	70.00%	80.00%	NN
Wrist	Lateral	normRGB-lum	Soft-max, r = l	89.65%	86.67%	92.85%	NN

The above table shows the best classification result for different body parts using Partek Discovery Suite. There were multiple experiments that provide the same results, the one with bigger data set was considered. The reason behind running experiment with Partek was to see if any pattern classification methods that were not available in CVIP-FEPC would provide better results with different data normalization methods. The results obtained from Partek were almost identical to those from CVIP-FEPC; in some cases one or two images being misclassified. This shows that the pattern classification algorithms that are available in CVIP-FEPC are sufficient for the classification purpose of this research study.

The next tools that was used for pattern classification was an artificial neural network (ANN). The image were divided into training and test set randomly to be used by ANN as shown in table.

Table 50: Number of images in different subgroups for ANN pattern classification method (red represents the group not being considered)

Body Part	Anterior	Lateral	Posterior
Elbow/Knee	**Training Set** Cancer = 10 No cancer= 10	**Training Set** Cancer = 15 No cancer= 15	**Training Set** Cancer = 8 No cancer= 9
	Test Set Cancer = 10 No cancer=11	**Test Set** Cancer = 14 No cancer=16	**Test Set** Cancer = 9 No cancer=8
Full Limb	**Training Set** Cancer = 3 No cancer= 3	**Training Set** Cancer = 7 No cancer= 9	Cancer = 2 No cancer=2
	Test Set Cancer = 2 No cancer=2	**Test Set** Cancer = 9 No cancer=8	
Shoulder Hip	Cancer = 3 No cancer=2	**Training Set** Cancer = 10 No cancer= 10	Cancer = 3 No cancer=1
		Test Set Cancer = 10 No cancer=10	
Wrist	**Training Set** Cancer = 6 No cancer= 5	**Training Set** Cancer = 7 No cancer= 7	**Training Set** Cancer = 3 No cancer= 4
	Test Set Cancer = 6 No cancer=6	**Test Set** Cancer = 8 No cancer=7	**Test Set** Cancer = 4 No cancer= 4

The features that were extracted using CVIP-FEPC were used for pattern classification. The features that were not normalized were used for this purpose. Principal component analysis was performed on all the features and only those principal components that contain 98% of variance were considered. The network was then trained using the training samples. Various plots along with MSE and percentage errors were used to evaluate how correctly the network is trained which are confusion matrix, receiver output characteristic curve and error histogram. The confusion matrix is used to evaluate the overall success rate, sensitivity, and specificity. Large values for each of them represent better result. A ROC curve is a plot between sensitivity and (1- specificity). A low value of MSE and percentage error signifies better training. The trained network was then used to classify the test samples.

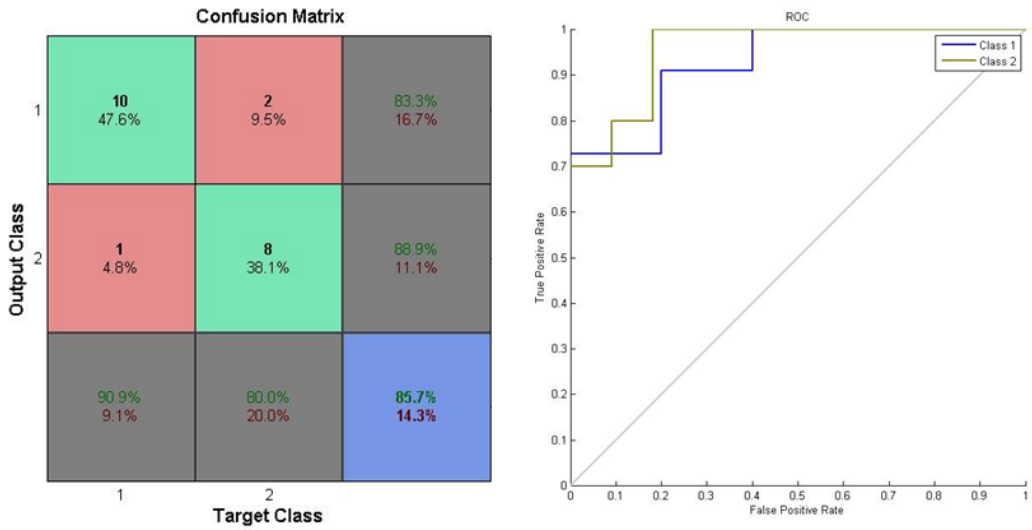

Figure 27: Sample plot showing Receiver output characteristics (ROC) curve (right) and confusion matrix (left).

The above figure show sample confusion matrix which specify how many samples were classified correctly and how many of them were misclassified based on which different success measure can be calculated. The ROC curve is a curve between true positive rate and false positive rate and a best result means a line of slope 1.

The table shows the results from ANN for different body parts for original and color normalized groups.

Table 51: Classification results Elbow/Knee region with ANN pattern classification method.

Elbow/Knee	Anterior (Cancer=20 Nocancer=21)	Color Normalization	Success Rate	Sensitivity	Specificity
		Orig	71.40%	70.00%	72.72%
		Lum	71.40%	80.00%	63.63%
		normGrey	85.70%	70.00%	100%
		normRGB	85.70%	80.00%	90.90%
		normRGB-lum	66.70%	50.00%	81.81%
	Lateral (Cancer=29 Nocancer=31)		Success Rate	Sensitivity	Specificity
		Orig	56.70%	42.85%	68.75%
		Lum	53.30%	23.07%	81.25%
		normGrey	63.30%	64.28%	62.50%
		normRGB	73.30%	64.28%	81.25%
		normRGB-lum	60.00%	100.00%	25.00%
	Posterior (Cancer=17 Nocancer=17)		Success Rate	Sensitivity	Specificity
		Orig	63.30%	66.67%	80.95%
		Lum	76.70%	66.67%	80.95%
		normGrey	63.30%	22.23%	80.95%
		normRGB	73.30%	55.56%	80.95%
		normRGB-lum	70%	44.45%	80.95%

Table 52: Classification results Full Limb region with ANN pattern classification method.

Full Limb	Anterior (Cancer=5 Nocancer=5)	Color Normalization	Success Rate	Sensitivity	Specificity
		Orig	100.00	100.00	100.00
		Lum	75.00	100.00	50.00
		normGrey	75.00	100.00	50.00
		normRGB	50.00	50.00	50.00
		normRGB-lum	75.00	50.00	100.00
	Lateral (Cancer=16 Nocancer=17)		Success Rate	Sensitivity	Specificity
		Orig	60.00	25.00	100.00
		Lum	66.70	62.50	71.42
		normGrey	66.70	62.50	71.42
		normRGB	66.70	50.00	85.71
		normRGB-lum	60.00	50.00	71.42

Table 53: Classification results Shoulder/Hip region with ANN pattern classification method.

Shoulder/Hip	Lateral (Cancer=20 Nocancer=20)	Color Normalization	Success Rate	Sensitivity	Specificity
		Orig	60.00	80.00	40.00
		Lum	70.00	70.00	70.00
		normGrey	60.00	60.00	60.00
		normRGB	65.00	50.00	80.00
		normRGB-lum	65.00	80.00	50.00

Table 54: Classification results Wrist region with ANN pattern classification method.

Wrist	Anterior (Cancer=12 Nocancer=11)	Color Normalization	Success Rate	Sensitivity	Specificity
		Orig	75.00%	66.67%	83.33%
		Lum	58.30%	33.33%	83.33%
		normGrey	66.70%	83.33%	50.00%
		normRGB	58.30%	66.67%	50.00%
		normRGB-lum	66.70%	50.00%	83.33%
	Lateral (Cancer=15 Nocancer=14)		Success Rate	Sensitivity	Specificity
		Orig	60.00%	25.00%	100.00%
		Lum	66.70%	62.50%	71.42%
		normGrey	66.70%	62.50%	71.42%
		normRGB	66.70%	50.00%	85.71%
		normRGB-lum	60.00%	50.00%	71.42%
	Posterior (Cancer=7 Nocancer=8)		Success Rate	Sensitivity	Specificity
		Orig	75.00%	50.00%	100.00%
		Lum	75.00%	100.00%	50.00%
		normGrey	75.00%	75.00%	75.00%
		normRGB	75.00%	75.00%	75.00%
		normRGB-lum	62.50%	25.00%	100.00%

Table 55: Best classification results for different body parts from ANN

Body Part	Camera View	Color Normalization	Success Rate	Sensitivity	Specificity
Elbow Knee	Anterior	normRGB	85.7%	80.00%	90.00%
Full Limb	Anterior	Orig	100%	100%	100%
Shoulder/Hip	Lateral	lum	70%	70%	70%
Wrist	Posterior	normRGB	75%	75%	75%

The table above shows the best results for different body parts from artificial neural network. The result shows 100% success rate with sensitivity of 100% and specificity of 100% for full limb region with anterior view. This group has also produced the best result from CVIP-FEPC. However it is also to be considered the fact that this is the smallest group among all the experiments.

A comparison between the best classification result for different body parts with three different pattern classification tools are shown by following figures.

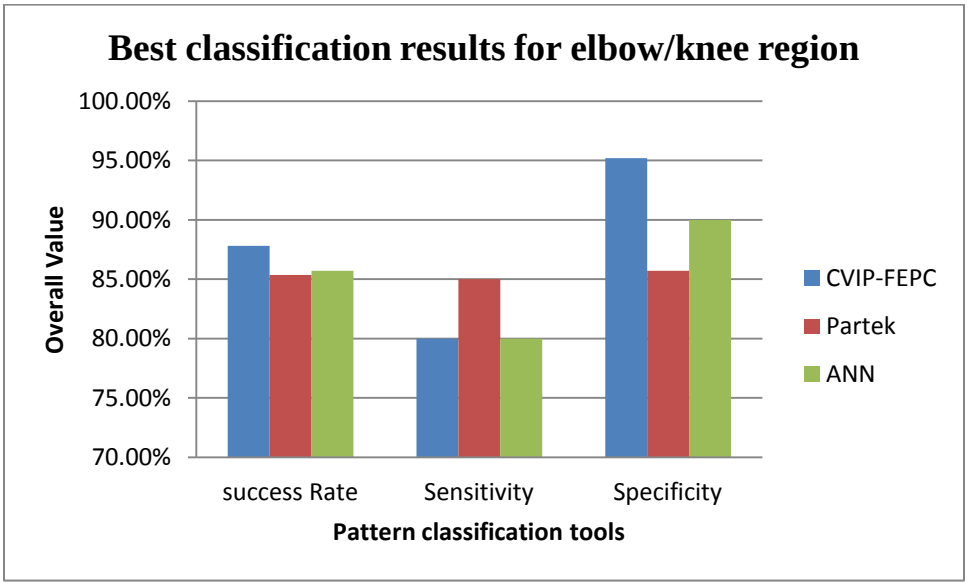

Figure 28: Overall success rate, sensitivity and specificity from best classification results from different pattern classification tools for elbow/knee region

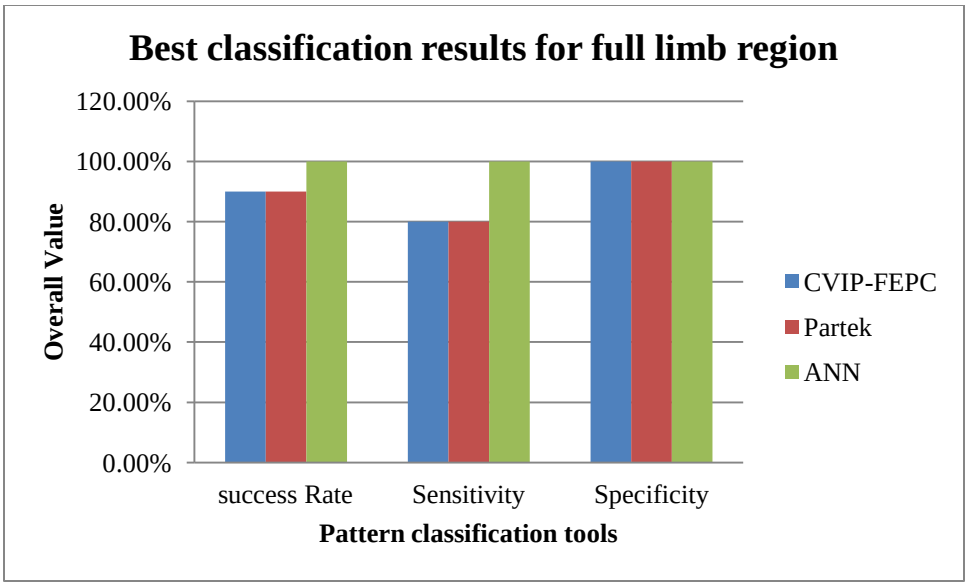

Figure 29: Overall success rate, sensitivity and specificity from best classification results from different pattern classification tools for full limb region.

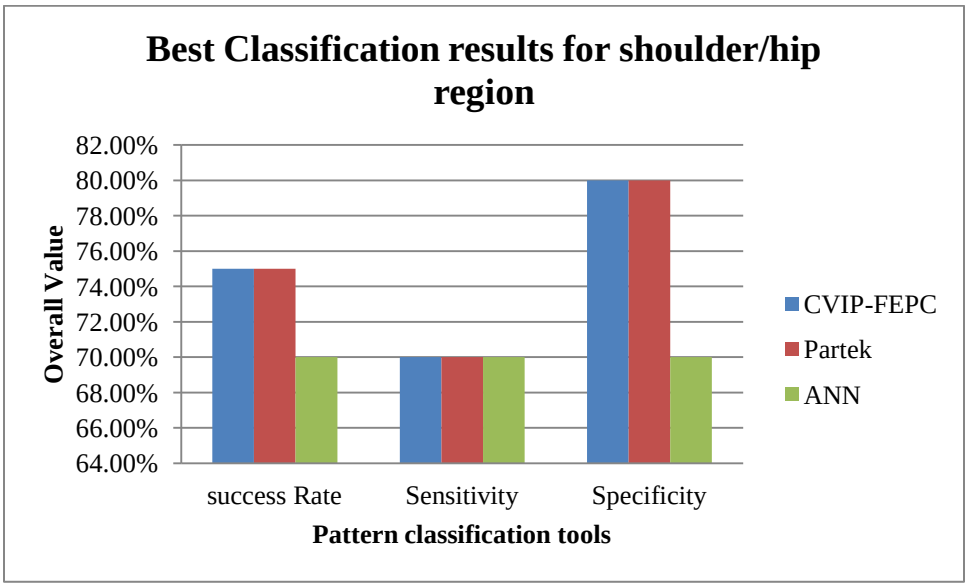

Figure 30: Overall success rate, sensitivity and specificity from best classification results from different pattern classification tools for shoulder/hip region.

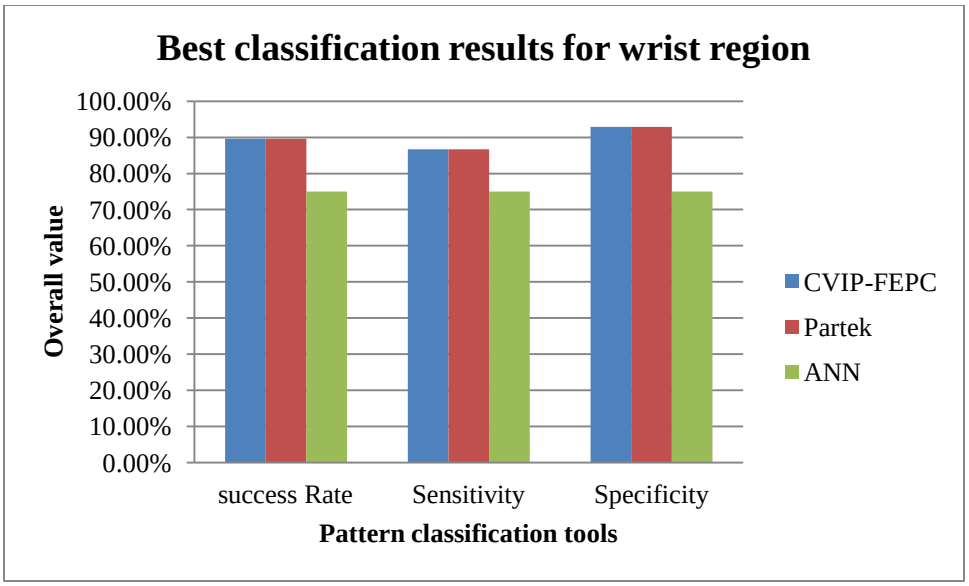

Figure 31: Overall success rate, sensitivity and specificity from best classification results from different pattern classification tools for wrist region.

From figures 28-31, we see that the result obtain from CVIP-FEPC and Partek Discovery Suite are identical while the results from ANN varied. For example, with the ANN the elbow/knee results were about the same, the full limb 10% better, shoulder/hip about 5% worse, and the wrist region with the ANN about 15% worse than with the CVIP-FEPC or Partek which used nearest neighbor classification.

CHAPTER 6
SUMMARY AND CONCLUSION

This research investigates using thermographic imaging as a pre-screening tool for the detection of canine bone cancer. Historically thermograms were analyzed either by observation by a specialist or statistical analysis of temperature data. Here, a computer based tool was developed and used to automate the classification with computer vision and image processing techniques combined with pattern classification methods. Texture features, spectral features and histogram features were extracted from thermographic images and used to classify the images as normal or abnormal.

The research was done in four stages. Experiments in the first stage consist of images from 34 dogs of which 140 were normal and 141 as abnormal. Experiments were performed with original as well as color normalized images. The first stage experiment was done using CVIP-FEPC and the highest classification success rate achieved was 64.06% which is not acceptable.

Division of images based on various factors such as hair type, body parts, limb types, body area, and camera views was performed for the second stage of experiment. The idea of dividing the images considering all these factors was to make the data sets more homogenous thus increasing the overall success rate. Dividing the images based on these factors and running experiment with CVIP-FEPC produced a better result compared to the result from first stage of experiment. Dividing images based on hair types did not show significant improvements in the results which conclude that hair might not be an important factor for thermographic image analysis. However a strong conclusion cannot be made as the data set was not completely homogeneous and images from various body parts, camera view, gender, breed and size of dogs were still present.

A huge improvement in the result was achieved after dividing image based on camera view. A overall success rate of 82.60% with sensitivity of 91.67% and specificity of 72.73% was achieved by anterior view for forelimb. Similarly for hindlimb success rate of 90.90% with sensitivity of 90.91% and specificity of 90.91% was achieved with anterior view. This result shows that division of images based on camera view is important factor to consider. So at the

third stage after dividing images based on body parts, a further division was made based on camera views. A highest classification success rate of 90.00% with sensitivity of 100% and specificity of 80% was achieved for full limb with anterior camera view and normRGB-lum as color normalization method. The features used, data normalization methods, and pattern classification methods used were different for individual experiment and a single algorithm representing all the experiments could not be made. However after reviewing the result, we see that nearest neighbor as important pattern classification methods softmax scaling as important data normalization methods. The camera view, and color normalization methods were dependent on body parts, however normRGB and normRGB-lum was mostly for best classification. The result obtained from this method was further evaluated using other pattern classification tools such as Partek Discovery suite and artificial neural network.

The result obtained from partek was almost identical with the result obtained from CVIP-FEPC signifying the importance of pattern classification algorithms available in CVIP-FEPC. The result after performing artificial neural network also shows a considerable result. A success rate from 70% to 100% was achieved with sensitivity from 70% to 100% and specificity from 70% to 100% was achieved for different body parts. After comparing the results from three pattern classification tools we see that the result obtain from CVIP-FEPC and Partek Discovery Suite are identical while the results from ANN varied. For example, with the ANN the elbow/knee results were about the same, the full limb 10% better, shoulder/hip about 5% worse, and the wrist region with the ANN about 15% worse than with the CVIP-FEPC or Partek which used nearest neighbor classification.

The overall results indicate the feasibility of using thermographic imaging as a pre-screening tool for detection of bone cancer in dogs. A complete and homogeneous data set is also important factor for classifying thermograms.

CHAPTER 7
SUGGESTION AND FUTURE WORK

In this research study experiments with different body parts, camera views and color normalization methods were performed and results analyzed in different stages. The images used in this research were not homogeneous and were from varieties of breed, size and length of disease first confirmed. These facts highly influence the nature and pattern of thermographic images. Experiments dividing images based on all these factors were not conducted due to limited sample size. More investigation on these can be done with more homogeneous data sets. For each experimental setup, color normalization was done separately for normal and abnormal data sets. Further investigation can be done with combined color normalization preliminary result of which is in appendix B. One of the objectives of this research study was also to investigate which features are most useful for classification purpose. More features can be investigated from literature and can be implemented. The research uses fundamental part of artificial neural network. A more detail research can be done using artificial neural network and genetic algorithms.

The result obtained from this result study is being used for another research that is still in progress at CVIP lab called clinical veterinary application. This application will use the findings of this research to classify new unknown thermograms as normal or abnormal.

REFERENCES

[1] Emanuela Morello, Marina Martano, Paolo Buracco "Biology, diagnosis and treatment of canine appendicular osteosarcoma: Similarities and differences with human osteosarcoma" Vet 189, 268-277(2011).

[2] Liptak, JM, WS Dernell, N Ehrhart, and SJ Withrow, "Canine appendicular osteosarcoma: diagnosis and palliative treatment." Compend Cont Educ Pract Vet 3:172-185, 2004.

[3] Liptak JM, "Canine Appendicular Osteosarcoma: Curative-Intent Treatment" Compendium on Continuing Education for the Practicing Veterinarian 26(3): 186-196, 2004

[4] Rybak, L., & Rosenthal, D, "Radiological imaging for the diagnosis of bone metastases", THE QUARTERLY JOURNAL OF NUCLEAR MEDICINE AND MOLECULAR IMAGING , 45, 53-64, 2001

[5] Arnulf Oppelt, " Imaging system for medical diagnostics, fundamentals, technical solutions and application for system applying ionizing radiation, nuclear magnetic resonance and ultrasound", Publicis corporate publishing,2005

[6] S.G. Burnay, T.L. Williams, C.H. Jones, "Applications of Thermal Imaging", IOP Publishing Ltd., Philadelphia,1988

[7] Catherine A. Loughin, DVM, and Dominic J. Marino, DVM, "Evaluation of thermographic imaging of the limbs of healthy dogs" American journal of veterinary research, 2007, American Veterinary Medical Association (AVMA).

[8] E.F.J Ring, "The historical development of temperature measurement in medicine", Infrared physics & technology 49, 297-301, 2007

[9] R.B Barnes, " Thermography of human body ", Science 140, 870-877, 1963

[10] A. Jung, J Zuber, F. Ring, " A case book of infrared imaging in clinical Medicine", MedPress, 2003

[11] A.L. Schaefer, N.J. Cook, C. Bench, J.B. Chabot, J. Colyn, T. Liu, E.K. Okine, M. Stewart, J.R. Webster, " The non- invasive and automated detection of bovine respiratory disease onset in receiver calves using infrared thermography", Research in veterinary science 93, 928-935, 2010

[12] Stubsjøen SM1, Flø AS, Moe RO, Janczak AM, Skjerve E, Valle PS, Zanella AJ. "Exploring non-invasive methods to assess pain in sheep", Physiology and Behavior 98, 640-648, 2009

[13] Stewart M. Webster JR, Verkerk GA, Schaefer AL, Colyn JJ, Stafford KJ, "Non-invasive measurement of stress in dairy cows using infrared thermography", Physiology and Behavior, 92,520-5, 2007

[14] Wan-Tae Kim, Min-Su Kim, Sun Young Kim, Kang-Moon Seo, Tchi-Chou Nam, " Use of digital infrared thermography on experimental spinal cord compression in dogs", Journal of Veterinary Clinics 22(4): 302-308, 2005

[15] Heath AM, Pugh DG, Sartin EA, Navarre B, Purohit RC, "Evaluation of the safety and efficacy of testicular biopsies in llamas" 58(6), 1125-30(2002).

[16] Spire MF, Drouillard JS, Galland JC, "Use of infrared thermography to detect inflammation caused by contaminated growth promotant ear implants in cattle" J Am Vet Med Assoc 215,1320–1324(1999).

[17] Colak A, Polat B, Okumus Z, "Short communication: early detection of mastitis using infrared thermography in dairy cows" J Dairy Sci 91,4244–4248(2008).

[18] Rainwater-Lovett K, Pacheco JM, Packer C, "Detection of foot-and-mouth disease virus infected cattle using infrared thermography" Vet J 180,317–324(2009).

[19] Stewart M, Webster JR, Verkerk GA, "Non-invasive measurement of stress in dairy cows using infrared thermography" Physiol Behav 92, 520–525(2007).

[20] Schaefer AL, Cook NJ, Church JS, "The use of infrared thermography as an early indicator of bovine respiratory disease complex in calves" Res Vet Sci 83, 376–384(2007).

[21] Purohit RC, Use of thermography in veterinary medicine, Rehabilitation Medicine and Thermography, Impress Publications(2008).

[22] Stewart M, Webster JR, Schaefer AL, Cook NJ, Scott SL, " Infrared thermography as a non-invasive tool to study animal welfare" Animal Welfare 14(4), 319-325(2005).

[23] Tunley BV, Henson FMD, "Reliabilty and repeatability of thermographic examination and the normal thermographic image of the thoracolumbar region in the horse" Equine Vet J 36,306–312(2004).

[24] Head JF, Elliot RL, "Infrared imaging: making progress in fulfilling its medical promise" IEEE Eng Med Biol Mag 21,80–85(2002).

[25] Gautherie M, Haehnel P, Walter J, "Thermovascular changes associated with in situ and minimal breast cancers" J Reprod Med 32,833–842(1987).

[26] S.C. Fok, E.Y.-K. Ng, K. Tai, "Early detection and visualization of breast tumor with thermogram and neural network" Journal of Mechanics in Medicine and Biology 2 (2), 185–196(2002).

[27] S.C. Fok, E.Y.-K. Ng, G.L. Thimm, "Developing case-based reasoning for discovery of breast cancer" Journal of Mechanics in Medicine and Biology 3 (3–4), 231–246(2003).

[28] Ng EY, Ung LN, Ng FC, Sim LS," Statistical analysis of healthy and malignant breast thermography" J Med Eng Technol 25(6),253-63(2001).

[29] E.Y.-K. Ng, S.C. Fok, "A framework for early discovery of breast tumor using thermography with artificial neural network" The Breast Journal 9 (4), 341–343(2003).

[30] Gratt BM, Sickles EA, Wexler CE "Thermographic characterization of osteoarthrosis of the temporomandibular joint", J Orofac Pain 7,345–353(1993).

[31] Verheye S, DeMeyer GRY, Krams R, "Intravascular thermography: immediate functional and morphological vascular findings" Eur Heart J 25,158–165(2004).

[32] Rich PB, Dulabon GR, Doullet CD, "Infrared thermography: a rapid, portable, and accurate technique to detect experimental pneumothorax" J Surg Res 120,163–170(2004).

[33] Doman I, IllesT "Thermal analysis of the human intervertebral disc" J Biomech Biophys Methods 61,207–214(2004).

[34] Use of digital infrared thermography on experimental spinal cord compression in dogs, Department of veterinary Surgery; college of vetenery medicine, Seoul national university.

[35] Purohit RC, Carson RL, Riddell MG, "Peripheral neurogenic thermogenic thermoregulation of the bovine scrotum" Thermol Int 17,138–142(2007).

[36] Rainwater-Lovett K, Pacheco JM, Packer C, "Detection of foot-and-mouth disease virus infected cattle using infrared thermography" Vet J 180,317–324(2009).

[37] Stewart M, Webster JR, Verkerk GA, "Non-invasive measurement of stress in dairy cows using infrared thermography" Physiol Behav 92,520–525(2007)

[38] William Lawson, David BenEliyahu, Linda Meinken, Joseph Chernilas, Howard Novotny, Peter Cohn, John Dervan, " Infrared thermography in the detection and management of coronary artery disease" The American Journal of Cardiology 72(12), 894–896(1993).

[39] J.P. Brooks, W.B. Perry, A.T. Putnam, R.E. Karulf, "Thermal imaging in the detection of bowel ischemia" Dis. Colon. Rectum 43 (9), 1319–1321(2000).

[40] Bob Berry, “A combined Approach for using thermography for the detection of diabetes mellitus”, Thermosense: Thermal Infrared Applications XXXVI, 2014

[41] Zivcak J., Madarasz L., Hudak R., “ Application of medical thermography in the diagnostics of carpal tunnel syndrome”, 12th IEEE international symposium on computational intelligence and informatics, 2011

[42] Carolin Hildebrandt, Christian Raschner, Kurt Ammer, “An overview of recent application of medical infrared thermography in sports medicine in Austria”, Sensors, 10(2), p4700, 2010

[43] Nikola Borojevic, Darko Kolaric, Simeon Grazio, Frane Grubisic, Svetlana Antonini, Iskra Alexandra Nola, Zeljko Herceg, " Thermography of rheumatoid arthritis and osteoarthritis", Conference Proceedings ELMAR, 293- 295, 2011

[44] A. Merla, G. L. Romani, "Functional Infrared Imaging in Medicine: A Quantitative Diagnostic Approach ", Proceedings of the 28th IEEE EMBS Annual International Conference, 2006

[45] E F J Ring, K Ammer "Infrared thermal imaging in medicine", Physiol. Meas. 33 R33, 2012

[46] William C. Amalu, " A review of breast thermography", international academy of breast thermography

[47] S.C. Fok, E.Y.-K. Ng, K. Tai, Early detection and visualization of breast tumor with thermogram and neural network, Journal of Mechanics in Medicine and Biology 2 (2) (2002) 185–196.

[48] C. Gros, M. Gautherie, Breast thermography and cancer risk prediction, Cancer 45 (1980) 51–56.

[49] J. Kerr, Review of the effectiveness of infrared thermal imaging (thermography) for population screening and diagnostic testing of breast cancer, New Zealand Health Technology Assessment (NZHTA) Tech. Brief Series 3 (3), 2004,

[50] E.Y.-K. Ng, Y. Chen, L.N. Ung, "Computerized breast thermography: Study of image segmentation and temperature cyclic variations", Int. J. Med. Eng. Technol. 25 (1) (2001) 12–16.

[51] E.Y.-K. Ng, Y. Chen, "Segmentation of breast thermogram: Improved boundary detection with modified snake algorithm", Journal of Mechanics in Medicine and Biology 6 (2) (2006) 123–136.

[52] Jones B., Plassman P.,"Computational approaches to image processing for improved interpretation and analysis", IEEE Eng. in Medicine and Biology, v. 21, 6, 2002, 41 - 48.

[53] Jakubowska T., Wiecek B., Wysocki M., Drews-Peszynski C., "Thermal signatures for breast cancer screening comparative study", Proc. IEEE EMBEC, Cancun, 2003, 1117–20

[54] Qi H., Kuruganti P.T., Liu Z., "Early detection of breast cancer using thermal texture maps", IEEE Int. Symp. On Biomedical Imaging, Washington DC, 2002, 309 – 312.

[55] Szu H., Kopriva I., Hoekstra P., Diakides N., Diakides M., Buss J., Lupo J., "Early Tumor Detection by Multiple Infrared Unsupervised Neural Nets fusion", Proc. IEEE EMBC, Cancun, 2003, 1133 – 1136.

[56] J. Koay, C. Herry, M. Frize, " Analysis of breast thermography with an artificial neural network", Engineering in Medicine and Biology Society, IEMBS '04. 26th Annual International Conference of the IEEE ,2004.

[57] L.J. Jiang, E.Y.K. Ng, W.Y. Yau, S. Wu, X.D. Jiang, A.C.B. Yeo, "A perspective on medical IR imaging", Int. J. Med. Eng. Technol. 29 (6) 257–267, 2005.

[58] E.Y.-K. Ng, S.C. Fok, "A framework for early discovery of breast tumor using thermography with artificial neural network", The Breast Journal 9 (4) 341–343, 2003.

[59] E.Y.-K. Ng, E.C. Kee, "Advanced integrated technique in breast cancer thermography", Int. J. Med. Eng. Technol. 32 (2) 103–114, 2008.

[60] B. Wiecek, M. Strzelecki, T. Jakubowska, M. Wysocki, C. Drews-Peszynski, "Advanced thermal image processing, in: Biomedical Engineering Handbook", CRC Press, 2006

[61] E.Y.-K. Ng, S.C. Fok, Y.C. Peh, F.C. Ng, L.S.J. Sim, "Computerized detection of breast cancer with artificial intelligence and thermograms", Int. J. Med. Eng. Technol. 26 (4) (2002) 152–157.

[62] E.Y.-K. Ng, S.C. Fok, "A framework for early discovery of breast tumor using thermography with artificial neural network", The Breast Journal 9 (4) (2003) 341–343.

[63] Meditherm Inc. Webpage, http://www.meditherm.com/mms_default.htm (last accessed December 2014)

[64] S Subedi, SE Umbaugh, J Fu, DJ Marino, CA Loughin, "Thermographic Image Analysis as a Pre-screening Tool for the Detection of Canine Bone Cancer", Applications Conference: Applications of Digital Signal Processing XXXVII, August, 2014, Proceedings of SPIE Vol. 9217.

[65] CVIPtools developers website, http://www.cviptools.ece.siue.edu (last accessed December 2014)

[66] S.E. Umbaugh, P. Solt, "Veterinary thermographic image analysis, data and temperature normalization", SIUE CVIP Laboratory report, 4878-3(2008).

[67] Partek Documentation, http://www.partek.com (last accessed December 2014)

[68] Matlab Documentation, http://www.mathworks.com/help/matlab/ (last accessed December 2014)

[69] Burke, H.B., Goodman, P.H., Rosen, D.B., Henson, D.E., Weinstein, J.N., Harrell, F.E., Marks, J.R., Winchester, D.P & Bostwick, D.G, "Artificial neutral network improve the accuracy of cancer survival prediction," Cancer, vol.79, 1997, pp.857-862.

[70] Umbaugh, E Scott [Digital Image Processing and Analysis: Human and Computer Vision Applications with CVIPtools], The CRC Press, Boca Raton, FL(2010).

[71] Umbaugh, E S., Subedi Samrat (Jan 2014), "Veterinary Thermographic Image Analysis". Project Number 7-64878, Report Number 4878-24, January, 2014.

[72] Umbaugh, E S., Fu Jiyuan, Subedi Samrat (May 2014), "Veterinary Thermographic Image Analysis". Project Number 7-64878, Report Number 4878-25, May, 2014

APPENDIX A

SAMPLE FEATURE FILE FROM CVIP-FEPC

CVIPtools feature file for image with 1 band
1. Image name
2. Object's row coordinate
3. Object's column coordinate
4. Histo_Mean
5. Histo_Standard_Deviation
6. Histo_Skew
7. Histo_Energy
8. Histo_Entropy
9. Texture energy average (Texture Distance: 7 IncludeZeroPairs: False)
10. Texture energy range
11. Inertia average (Texture Distance: 7 IncludeZeroPairs: False)
12. Inertia range
13. Correlation average (Texture Distance: 7 IncludeZeroPairs: False)
14. Correlation range
15. Inverse diff average (Texture Distance: 7 IncludeZeroPairs: False)
16. Inverse diff range
17. Texture entropy average (Texture Distance: 7 IncludeZeroPairs: False)
18. Texture entropy range
19. Spectral_DC
20. Ring1
21. Ring2
22. Ring3
23. Sector1
24. Sector2
25. Sector3
*** END OF HEADER; CLASS (optional) SHOWN AT THE END OF DATA ***

anddol022312ahl2-orig-lum.tif 38 60 145.452035 31.342084 -0.897725 0.116356 3.340977 0.033097 0.019380 1065.050415 566.144897 0.282357 0.404098 0.031846 0.012104 5.576961 0.743857 1975.262376 1.200347 0.009791 0.002157 0.848178 0.249194 0.114923 Nocancer

anddol022312ahr2-orig-lum.tif 11 213 145.117288 24.626762 0.807565 0.172516 2.752256 0.070867 0.024390 384.872803 182.906006 0.677234 0.155062 0.027409 0.008879 4.321560 0.399765 2623.416622 0.947612 0.007691 0.002083 0.753697 0.168643 0.035046 Cancer

bibbac061112ahll2-orig-lum.tif 29 55 151.089581 39.236330 0.017837 0.136563 3.165294 0.046497 0.010335 1555.272339 516.192383 0.490822 0.162808 0.021354 0.006421 5.171809 0.299712 976.148649 2.052026 0.022467 0.006441 1.254894 0.385473 0.440567 Cancer

bibbac061112ahrl2-orig-lum.tif 58 279 128.164815 31.694296 -1.530334 0.172972 2.794515 0.051503 0.026472 1111.878784 680.831726 0.336782 0.420064 0.037817 0.013398 4.830750 0.571784 71.374859 7.425415 0.101209 0.022248 6.154555 0.738383 0.655934 Nocancer

blarexa102312afl2-orig-lum.tif 0 46 149.780733 31.962905 -0.270046 0.156832 3.116580 0.052190 0.018772 1337.608154 686.481750 0.277958 0.391740 0.025575 0.010160 5.201586 0.640679 2987.645941 0.913492 0.014935 0.004014 0.768971 0.143224 0.020246 Nocancer

blarexa102312afr2-orig-lum.tif 12 242 151.798959 33.045486 0.286604 0.116475 3.331882 0.022267 0.008441 1779.156250 307.775269 0.202099 0.115746 0.032499 0.005363 6.076159 0.631219 228.842715 4.684866 0.055356 0.014656 3.599800 0.709979 0.445100 Cancer

bocree060812afl2-orig-lum.tif 0 32 141.885853 24.545088 -1.347938 0.185112 2.847068 0.055796 0.012938 655.592163 237.047852 0.246708 0.372800 0.044849 0.007769 4.980364 0.289816 580.225005 2.498117 0.025896 0.009179 1.858151 0.417605 0.257436 Nocancer

bocree060812aflr2-orig-lum.tif 4 199 66.787096 70.883253 1.020486 0.113554 3.443798 0.021370 0.005372 3963.607666 1558.995361 0.618901 0.137230 0.031688 0.002954 6.406884 0.303609 117.750117 5.935289 0.085170 0.023008 3.597351 1.791626 0.654491 Cancer

chewie111312ahl2-orig-lum.tif 0 52 152.492417 30.122043 0.301348 0.102145 3.385286 0.029924 0.016243 788.497559 603.697571 0.560574 0.346042 0.027022 0.009454 5.403100 0.772535 1554.603994 1.495257 0.011205 0.002743 1.146869 0.212311 0.150026 Cancer

chewie111312ahr2-orig-lum.tif 0 137 149.975740 29.110772 0.704548 0.134618 3.148932 0.044897 0.018852 959.041199 512.842407 0.435945 0.299564 0.025466 0.008152 5.291750 0.716077 3911.376727 0.736026 0.006537 0.001608 0.494888 0.182616 0.066667 Nocancer

cioyel091012afl2-orig-lum.tif 13 93 110.493007 49.651364 -0.684705 0.159068 2.969741 0.047573 0.014845 1272.519165 732.617554 0.742564 0.148257 0.033738 0.001971 5.131323 0.463267 823.240573 1.793437 0.015894 0.004899 1.328719 0.309935 0.175577 Nocancer

cioyel091012afr2-orig-lum.tif 21 223 146.112306 27.990392 0.075039 0.126060 3.241796 0.035866 0.009694 964.317261 378.896240 0.331672 0.260682 0.032882 0.004900 5.593468 0.520586 1285.404557 1.594481 0.014261 0.003689 1.247898 0.232874 0.131659 Cancer

danlil060211ahL2TIBIA-orig-lum.tif 94 188 160.425607 29.126353 -0.190651 0.193890 2.716778 0.076606 0.020534 910.200439 466.273743 0.458447 0.283537 0.018316 0.005741 4.551444 0.509089 1260.558781 1.816825 0.013942 0.002894 1.057762 0.557617 0.218282 Cancer

danlil060211ahr2TIBIA-orig-lum.tif 109 188 141.063315 25.809954 0.601820 0.141186 3.030733 0.041146 0.019865 786.783691 444.407959 0.389958 0.348942 0.032835 0.009345 5.180480 0.586083 15245.692783 0.086651 0.003138 0.000547 0.072993 0.014550 0.002793 Nocancer

giache031212ahl2-orig-lum.tif 24 122 136.612073 28.019184 -1.954858 0.276019 2.319947 0.112883 0.027699 578.078674 259.668549 0.555240 0.214916 0.033991 0.008013 4.123277 0.374380 1401.153993 1.389963 0.008946 0.002618 0.744263 0.309441 0.347823 Nocancer

giache031212ahr2-orig-lum.tif 25 216 174.277552 30.027007 -0.625477 0.194681 2.559117 0.059368 0.013662 950.675293 341.893555 0.462712 0.194583 0.020035 0.004334 4.513374 0.311881 4991.611373 0.762272 0.005785 0.001891 0.454724 0.303341 0.011883 Cancer

grycod030612ahl2-orig-lum.tif 44 51 159.712789 33.022267 -0.390598 0.131887 3.205520 0.028334 0.018539 1465.671631 733.857605 0.253548 0.386270 0.029888 0.009183 5.757927 0.823078 805.099061 2.400892 0.027804 0.005926 2.011690 0.321052 0.101879 Nocancer

grycod030612ahr2-orig-lum.tif 62 250 165.295895 32.982598 -0.201519 0.119728 3.319688 0.027502 0.017594 1574.621094 839.840332 0.269977 0.394111 0.029039 0.010112 5.802194 0.811517 610.217245 2.945540 0.026209 0.007070 2.257546 0.436740 0.284533 Cancer

henrub052611afl2-orig-lum.tif 22 115 112.400156 55.954709 -0.387695 0.090603 3.668440 0.030341 0.010040 1171.822266 808.904602 0.800972 0.141333 0.025600 0.005672 5.730463 0.687464 2565.253402 0.877680 0.005530 0.001361 0.457022 0.377856 0.049693 Cancer

henrub052611afr2-orig-lum.tif 64 101 157.141560 41.982446 -1.286321 0.116631 3.387121 0.039093 0.015968 1184.095947 766.985107 0.517010 0.320954 0.023542 0.005301 5.253664 0.481771 1830.655773 1.455671 0.009567 0.002156 0.931312 0.412416 0.123666 Nocancer

hinkyl051712afll2-orig-lum.tif 40 59 127.627006 39.787552 -1.507280 0.177156 2.888703 0.059414 0.015297 953.366272 662.518799 0.664500 0.260493 0.040738 0.005015 4.833831 0.330005 537.145835 2.497432 0.017971 0.005491 1.794421 0.497483 0.228990 Cancer

hinkyl051712afrl2-orig-lum.tif 106 217 169.363006 22.778458 -1.218696 0.364150 1.783150 0.182146 0.031441 569.425659 481.199188 0.313030 0.664215 0.017159 0.004784 3.108780 0.261013 294.362569 4.477778 0.037423 0.009650 3.179825 0.728732 0.616294 Nocancer

hofjac122911AFLL2-orig-lum.tif 0 61 170.963447 28.700527 -0.596936 0.252543 2.279917 0.103124 0.023063 683.070190 213.475464 0.542394 0.174138 0.018720 0.005944 3.988137 0.280855 1546.335377 1.720746 0.011420 0.002857 1.398348 0.213617 0.123058 Nocancer

hofjac122911AFR2-orig-lum.tif 28 239 160.985904 32.936770 -0.445374 0.163835 2.992477 0.065597 0.010450 832.974609 398.336670 0.611695 0.182394 0.020235 0.003526 4.849378 0.322427 1510.180291 1.643816 0.011499 0.002647 1.274283 0.284797 0.098882 Cancer

kohzoe072412ahl2-orig-lum.tif 5 44 147.485066 26.984904 0.476787 0.287658 2.045295 0.122433 0.039904 695.224121 482.567261 0.492887 0.365578 0.017552 0.005484 3.597160 0.443389 727.586745 2.296038 0.023707 0.005545 1.624015 0.336426 0.364849 Cancer

kohzoe072412ahrl2-orig-lum.tif 35 246 156.203722 31.159311 0.312354 0.137667 3.067897 0.044853 0.027677 776.903748 585.448120 0.607718 0.291972 0.024357 0.010658 4.941395 0.692493 837.811682 2.283576 0.017504 0.004519 1.783330 0.370714 0.151554 Nocancer

mccpip062111antfemurleft-orig-lum.tif 5 46 128.283701 54.548457 -0.964862 0.090090 3.724122 0.020797 0.012985 1537.995361 937.416443 0.675976 0.214318 0.038526 0.008494 6.337073 0.716533 2242.284632 1.087352 0.010024 0.002052 0.933099 0.137358 0.028971 Nocancer

mcgbud111611afl2-orig-lum.tif 31 38 142.366454 30.059093 -1.442097 0.147001 2.962804 0.036007 0.022100 1262.705200 674.196838 0.152001 0.436772 0.038301 0.013938 5.249287 0.698168 739.714498 2.177827 0.048033 0.007924 2.091612 0.124341 0.017831 Nocancer

mcgbud111611afr2-orig-lum.tif 27 304 121.579394 51.346697 -0.610750 0.076781 3.867923 0.012338 0.011245 2650.983887 1151.928345 0.343869 0.311291 0.037786 0.016377 6.899268 0.813388 92.453319 6.822653 0.099168 0.027632 5.778527 0.839217 0.331709 Cancer

meinik090412afl22-orig-lum.tif 23 90 142.447147 15.182804 0.918219 0.269622 2.306624 0.123132 0.058455 322.629425 194.058868 0.291593 0.391180 0.032843 0.015883 3.884921 0.618155 733.354598 2.139066 0.016580 0.004257 1.604037 0.308921 0.246945 Nocancer

meinik090412afl2-orig-lum.tif 28 53 142.689150 16.390271 0.514155 0.215183 2.534259 0.078912 0.037101 441.601013 192.627747 0.142839 0.328334 0.041867 0.018074 4.392478 0.615197 2548.875490 0.915320 0.013061 0.003313 0.763788 0.131600 0.036307 Nocancer

meinik090412afr22-orig-lum.tif 27 212 153.575107 30.469394 0.200587 0.217005 2.420538 0.093440 0.040546 643.471558 482.649048 0.661063 0.245331 0.015270 0.007226 3.944913 0.608294 1158.707638 1.828400 0.012677 0.003469 1.346613 0.307973 0.189961 Cancer

meinik090412afr2-orig-lum.tif 25 276 171.962404 34.572271 -0.527443 0.228462 2.373553 0.090966 0.021356 935.252258 486.167358 0.626205 0.181578 0.015493 0.005062 3.944334 0.331360 314.258067 4.486562 0.046960 0.012547 3.190631 0.776732 0.578706 Cancer

oshkyl032012afll2-orig-lum.tif 67 55 147.975380 35.092417 -0.157541 0.105575 3.498974 0.027005 0.019245 1753.539185 721.135376 0.209244 0.318402 0.028571 0.010872 5.988122 0.814507 636.100029 2.562090 0.029029 0.007331 1.791948 0.420636 0.385867 Cancer

oshkyl032012afrl2-orig-lum.tif 93 203 145.299828 35.356408 -0.255902 0.121353 3.445994 0.036979 0.024607 1732.092407 1292.501709 0.193115 0.590654 0.031264 0.011744 5.885993 1.024641 324.741452 3.724005 0.036919 0.009193 2.791469 0.647528 0.331119 Nocancer

raacha032911ahl2-orig-lum.tif 47 134 112.296752 72.992893 0.003114 0.070170 3.997787 0.012326 0.005670 3686.174805 1760.562500 0.621707 0.175633 0.030253 0.002175 7.021055 0.563185 308.536815 4.006018 0.030838 0.010065 2.391004 1.195872 0.460046 Cancer

raacha032911ahr2-orig-lum.tif 12 218 143.260626 31.499185 -0.231234 0.111113 3.420858 0.022595 0.013371 1468.976807 730.881531 0.210326 0.404028 0.033938 0.010218 6.106505 0.683774 2268.030168 1.064582 0.009569 0.002606 0.779539 0.186016 0.111202 Nocancer

silell073112ahl2-orig-lum.tif 80 70 62.568103 48.446903 0.564996 0.185513 2.687570 0.045028 0.008432 2354.961670 961.677246 0.501237 0.209005 0.030984 0.002577 5.033956 0.234897 82.139693 4.931264 0.067759 0.021955 3.497789 1.114416 0.408772 Nocancer

silell073112ahr2-orig-lum.tif 70 228 3.395180 15.777058 6.691726 0.782932 0.759726 0.075480 0.036486 3347.676514 3292.636963 0.151747 0.873736 0.032793 0.010703 4.276967 0.559797 0.518556 51.642681 0.834443 0.281545 42.941707 6.735911 3.081050 Cancer

Yumic042412afl2-orig-lum.tif 51 155 186.721484 29.393013 -1.306851 0.287600 2.315473 0.154261 0.038905 804.510376 387.427734 0.440213 0.275247 0.013342 0.005017 3.787555 0.399099 1930.428818 1.664235 0.010503 0.002781 1.249423 0.334007 0.094090 Nocancer

Yumic042412afr2-orig-lum.tif 38 203 165.543722 34.415356 -0.422001 0.205167 2.558411 0.094629 0.027701 788.555664 343.742798 0.673459 0.140507 0.012530 0.004108 4.013169 0.330870 2523.504696 1.205788 0.010457 0.002633 0.888570 0.277581 0.052726 Cancer

Sample individual experiment result file

CVIPtools feature file for image with 1 band
1. Image name
2. Object's row coordinate
3. Object's column coordinate
4. Histo_Entropy
*** END OF HEADER; CLASS (optional) SHOWN AT THE END OF DATA ***

*** PATTERN CLASSIFICATION HEADER ***
Test Type: Leave-One-Out
Classification Algorithm: K-nearest Neighbor k = 5
Data Normalization: Softmax Normalization r = 1
Distance Measure: Euclidean Distance
Feature File: C:\Users\Samrat\Desktop\New Research Bone Cancer\ElbowKnee\Anterior\lum\Result\Experiment1\FeatureFile1.txt
Normalized Training Set File: C:\Users\Samrat\Desktop\New Research Bone Cancer\ElbowKnee\Anterior\lum\Result\Experiment1\TrainSet1-SMax1.txt
Normalized Test Set File: C:\Users\Samrat\Desktop\New Research Bone Cancer\ElbowKnee\Anterior\lum\Result\Experiment1\TestSet1-SMax1.txt
Output File: C:\Users\Samrat\Desktop\New Research Bone Cancer\ElbowKnee\Anterior\lum\Result\Experiment1\Results1.1-KNN5-Euc-SMax1.txt

1. Image Name in Test Set
2. Object's row coordinate in Test Set
3. Object's column coordinate in Test Set
4. Class in Test Set
5. Class in Training Set
6. Value of Distance or Similarity Measure
*** END OF PATTERN CLASSIFICATION HEADER ***

anddol022312ahl2-orig-lum.tif 38 60 Nocancer Cancer 0.003304
anddol022312ahr2-orig-lum.tif 11 213 Cancer Nocancer 0.016976
bibbac061112ahll2-orig-lum.tif 29 55 Cancer Nocancer 0.006420
bibbac061112ahrl2-orig-lum.tif 58 279 Nocancer Cancer 0.016973
blarexa102312afl2-orig-lum.tif 0 46 Nocancer Nocancer 0.012785
blarexa102312afr2-orig-lum.tif 12 242 Cancer Nocancer 0.003303
bocree060812afl2-orig-lum.tif 0 32 Nocancer Nocancer 0.021268
bocree060812aflr2-orig-lum.tif 4 199 Cancer Nocancer 0.000747
chewie111312ahl2-orig-lum.tif 0 52 Cancer Nocancer 0.000647
chewie111312ahr2-orig-lum.tif 0 137 Nocancer Nocancer 0.012788
cioyel091012afl2-orig-lum.tif 13 93 Nocancer Nocancer 0.002822
cioyel091012afr2-orig-lum.tif 21 223 Cancer Cancer 0.029093
danlil060211ahL2TIBIA-orig-lum.tif 94 188 Cancer Nocancer 0.011533
danlil060211ahr2TIBIA-orig-lum.tif 109 188 Nocancer Nocancer 0.014968
giache031212ahl2-orig-lum.tif 24 122 Nocancer Nocancer 0.001440
giache031212ahr2-orig-lum.tif 25 216 Cancer Cancer 0.000264
grycod030612ahl2-orig-lum.tif 44 51 Nocancer Cancer 0.013897
grycod030612ahr2-orig-lum.tif 62 250 Cancer Cancer 0.004455
henrub052611afl2-orig-lum.tif 22 115 Cancer Cancer 0.051275

henrub052611afr2-orig-lum.tif 64 101 Nocancer Cancer 0.000648
hinkyl051712afll2-orig-lum.tif 40 59 Cancer Nocancer 0.016929
hinkyl051712afrl2-orig-lum.tif 106 217 Nocancer Nocancer 0.121902
hofjac122911AFLL2-orig-lum.tif 0 61 Nocancer Nocancer 0.008432
hofjac122911AFR2-orig-lum.tif 28 239 Cancer Nocancer 0.009238
kohzoe072412ahl2-orig-lum.tif 5 44 Cancer Nocancer 0.056688 NOTE: The k nearest samples have all different or all the same class names. Nearest neighbor operation performed.
kohzoe072412ahrl2-orig-lum.tif 35 246 Nocancer Nocancer 0.014971
mccpip062111antfemurleft-orig-lum.tif 5 46 Nocancer Cancer 0.015359
mcgbud111611afl2-orig-lum.tif 31 38 Nocancer Nocancer 0.002822
mcgbud111611afr2-orig-lum.tif 27 304 Cancer Cancer 0.027656
meinik090412afl22-orig-lum.tif 23 90 Nocancer Nocancer 0.002834
meinik090412afl2-orig-lum.tif 28 53 Nocancer Cancer 0.008980
meinik090412afr22-orig-lum.tif 27 212 Cancer Nocancer 0.033643
meinik090412afr2-orig-lum.tif 25 276 Cancer Nocancer 0.017633
oshkyl032012afll2-orig-lum.tif 67 55 Cancer Nocancer 0.017668
oshkyl032012afrl2-orig-lum.tif 93 203 Nocancer Cancer 0.000746
raacha032911ahl2-orig-lum.tif 47 134 Cancer Cancer 0.027487
raacha032911ahr2-orig-lum.tif 12 218 Nocancer Cancer 0.007863
silell073112ahl2-orig-lum.tif 80 70 Nocancer Cancer 0.011534
silell073112ahr2-orig-lum.tif 70 228 Cancer Nocancer 0.074798
Yumic042412afl2-orig-lum.tif 51 155 Nocancer Nocancer 0.001440
Yumic042412afr2-orig-lum.tif 38 203 Cancer Cancer 0.000264

*** STATISTICS ***
#: Class in the Test File
@: Class identified

#1. Nocancer
#2. Cancer

@1. Nocancer
@2. Cancer

	@1	@2	% Correct
#1	12	9	57.14%
#2	13	7	35.00%

Sample report file from Partek

Partek Inc. December 02 2014
www.partek.com 05:17:10 pm
Test Summary for "none.csv"
Report invoked from model selection

Summary

Variable to Predict	27. ClassName
# of Predictor Candidates	25
# of Samples	15
# of Models	7
Random Seed	10001
Data Order	Randomly reorder data
Model Selection Criterion	Correct Rate
Cross-Validation	1-level
Partitions	15

Data Partition Report

Pass #	Test Set Row # List
1	1
2	6
3	10
4	9
5	7
6	11
7	5
8	14
9	8
10	3
11	15
12	12
13	2
14	13
15	4

Variable Selection Parameters

Variable Selection Method	Manually Select Variables
Variables Used	8. Histo_Energy
	10. Texture Energy Average
	11. Texture Energy Range
	14. Correlation Average

	15. Correlation Range
	18. Texture Entropy Average
	19. Texture Entropy Range

Classification Parameters

Classification Method	K-Nearest Neighbor
Distance Measure	Euclidean
# of Neighbors (K)	1
	3
	5
Classification Method	Discriminant Analysis
Discriminant Function and Prior Probabilities	Linear with Equal Prior Probabilities
	Linear with Proportional Prior Probabilities
	Quadratic with Equal Prior Probabilities
	Quadratic with Proportional Prior Probabilities

Model Overall Scores

Model	Correct Rate	Normalized Correct Rate	Kappa	Matthews Correlation Coefficient	Area Under Curve
7 variables, Linear Discriminant Analysis with Equal Prior Probability	0.7333	0.7321	0.4643	0.4643	0.5000
7 variables, Linear Discriminant Analysis with Proportional Prior Probability	0.7333	0.7321	0.4643	0.4643	0.5000
7 variables, K-Nearest Neighbor with Euclidean distance measure and 1 neighbor	0.6667	0.6696	0.3363	0.3393	0.5000
7 variables, K-Nearest Neighbor with Euclidean distance measure and 3 neighbors	0.6000	0.5893	0.1818	0.1890	0.5000
7 variables, K-Nearest Neighbor with Euclidean distance measure and 5 neighbors	0.4667	0.4643	-0.0714	-0.0714	0.5000
7 variables, Quadratic Discriminant Analysis with Equal Prior Probability	0.1333	0.1250	-0.7568	-0.7638	0.5000
7 variables, Quadratic Discriminant Analysis with Proportional Prior Probability	0.1333	0.1250	-0.7568	-0.7638	0.5000

Confusion Matrix for the model "7 variables, Linear Discriminant Analysis with Equal Prior Probability"

Real\Predicted	Cancer	Nocancer
Cancer	5	2
Nocancer	2	6

Classification Summary for the model "7 variables, Linear Discriminant Analysis with Equal Prior Probability"

	# Per Class	Proportion	# Correct	# Errors	% Correct	% Error	Std. Error
Cancer	7	0.47	5	2	71.00	29.00	17.07%
Nocancer	8	0.53	6	2	75.00	25.00	15.31%
The Average					73.00	27.00	
Total	15	1	11	4	73.33	26.67	11.42%
Kappa=0.4643							

Confusion Matrix for the model "7 variables, Linear Discriminant Analysis with Proportional Prior Probability"

Real\Predicted	Cancer	Nocancer
Cancer	5	2
Nocancer	2	6

Classification Summary for the model "7 variables, Linear Discriminant Analysis with Proportional Prior Probability"

	# Per Class	Proportion	# Correct	# Errors	% Correct	% Error	Std. Error
Cancer	7	0.47	5	2	71.00	29.00	17.07%
Nocancer	8	0.53	6	2	75.00	25.00	15.31%
The Average					73.00	27.00	
Total	15	1	11	4	73.33	26.67	11.42%
Kappa=0.4643							

Confusion Matrix for the model "7 variables, Quadratic Discriminant Analysis with Equal Prior Probability"

Real\Predicted	Cancer	Nocancer
Cancer	0	7
Nocancer	6	2

Classification Summary for the model "7 variables, Quadratic Discriminant Analysis with

Equal Prior Probability"

	# Per Class	Proportion	# Correct	# Errors	% Correct	% Error	Std. Error
Cancer	7	0.47	0	7	0.00	100.00	0.00%
Nocancer	8	0.53	2	6	25.00	75.00	15.31%
The Average					12.50	87.50	
Total	15	1	2	13	13.33	86.67	8.78%
Kappa=-0.7568							

Confusion Matrix for the model "7 variables, Quadratic Discriminant Analysis with Proportional Prior Probability"

Real\Predicted	Cancer	Nocancer
Cancer	0	7
Nocancer	6	2

Classification Summary for the model "7 variables, Quadratic Discriminant Analysis with Proportional Prior Probability"

	# Per Class	Proportion	# Correct	# Errors	% Correct	% Error	Std. Error
Cancer	7	0.47	0	7	0.00	100.00	0.00%
Nocancer	8	0.53	2	6	25.00	75.00	15.31%
The Average					12.50	87.50	
Total	15	1	2	13	13.33	86.67	8.78%
Kappa=-0.7568							

Confusion Matrix for the model "7 variables, K-Nearest Neighbor with Euclidean distance measure and 1 neighbor"

Real\Predicted	Cancer	Nocancer
Cancer	5	2
Nocancer	3	5

Classification Summary for the model "7 variables, K-Nearest Neighbor with Euclidean distance measure and 1 neighbor"

	# Per Class	Proportion	# Correct	# Errors	% Correct	% Error	Std. Error
Cancer	7	0.47	5	2	71.00	29.00	17.07%
Nocancer	8	0.53	5	3	63.00	38.00	17.12%
The Average					67.00	33.50	
Total	15	1	10	5	66.67	33.33	12.17%
Kappa=0.3363							

Confusion Matrix for the model "7 variables, K-Nearest Neighbor with Euclidean distance measure and 3 neighbors"

Real\Predicted	Cancer	Nocancer
Cancer	3	4
Nocancer	2	6

Classification Summary for the model "7 variables, K-Nearest Neighbor with Euclidean distance measure and 3 neighbors"

	# Per Class	Proportion	# Correct	# Errors	% Correct	% Error	Std. Error
Cancer	7	0.47	3	4	43.00	57.00	18.70%
Nocancer	8	0.53	6	2	75.00	25.00	15.31%
The Average					59.00	41.00	
Total	15	1	9	6	60.00	40.00	12.65%
Kappa=0.1818							

Confusion Matrix for the model "7 variables, K-Nearest Neighbor with Euclidean distance measure and 5 neighbors"

Real\Predicted	Cancer	Nocancer
Cancer	3	4
Nocancer	4	4

Classification Summary for the model "7 variables, K-Nearest Neighbor with Euclidean distance measure and 5 neighbors"

	# Per Class	Proportion	# Correct	# Errors	% Correct	% Error	Std. Error
Cancer	7	0.47	3	4	43.00	57.00	18.70%
Nocancer	8	0.53	4	4	50.00	50.00	17.68%
The Average					46.50	53.50	
Total	15	1	7	8	46.67	53.33	12.88%
Kappa=-0.0714							

APPENDIX B

PRELIMINARY RESULT FROM COMBINED COLOR NORMALIZATION

Table 1: Classification success rate for Elbow/Knee for different camera view

Body Part	Camera View	Color Normalization	Success Rate	Sensitivity	Specificity
Elbow Knee	Anterior	Original	73.17%	70.00%	76.19%
		Lum	75.60%	80.00%	71.43%
		NormGrey	82.92%	80.00%	85.71%
		NormRGB	85.36%	80.00%	90.48%
		NormRGB-lum	85.36%	85.00%	85.71%
	Lateral	Original	60.00%	58.62%	61.29%
		Lum	68.33%	68.97%	67.74%
		NormGrey	65.00%	55.17%	74.19%
		NormRGB	70.00%	65.52%	74.19%
		NormRGB-lum	70.00%	68.97%	70.97%
	Posterior	Original	76.47%	70.59%	82.35%
		Lum	73.52%	58.24%	88.24%
		NormGrey	76.47%	76.47%	76.47%
		NormRGB	79.41%	76.47%	82.35%
		NormRGB-lum	73.52%	82.35%	64.71%

Table 2: Features, data normalization and pattern classification methods used for best classification for elbow/knee region.

Body Part	Camera View	Color Normalization	Features	Data Normalization	Pattern Classification
Elbow/ Knee	Anterior	Original	Texture Energy Texture Inv Diff	None	NN
		Lum	Texture Energy Texture Correlation Texture InvDiff Texture Entropy Histogram Mean Histogram StdDev Histogram Skew Histogram Energy Histogram Entropy	Soft-max, r = l	NN
		NormGrey	Texture Energy Histogram Skew Histogram Energy	Soft-max, r = l	NN
		NormRGB	Histogram Mean Histogram Stddev Histogram Skew	Soft-max, r = l	KNN5
		NormRGB-lum	Histogram Mean Histogram Skew	None	KNN5
	Lateral	Original	Histogram Stddev	Soft-max, r = l	NN
		Lum	Histogram Mean Histogram StdDev Histogram Energy Histogram Entropy	Soft-max, r = l	NN
		NormGrey	Texture Inertia Histogram StdDev	Soft-max, r = l	NN
		NormRGB	Texture Entropy Histogram Skew	Soft-max, r = l	NN
		NormRGB-lum	Histogram Mean Histogram Skew Histogram Energy	Standard Normal	NN

Elbow/ Knee	Posterior	Original	Histogram StdDev Histogram Energy	Standard Normal	KNN5
		Lum	Texture InvDiff Histogram Mean	Soft-max, r = l	KNN5
		NormGrey	Texture Inertia Texture InvDiff Histogram Mean Histogram StdDev Histogram Entropy	Soft-max, r = l	KNN5
		NormRGB	Texture InvDiff Testure Entropy Histogram StdDev	Soft-max, r = l	KNN5
		NormRGB-lum	Texture InvDiff Histogram StdDev Histogram Energy Histogram Entropy	Soft-max, r = l	KNN5

Table 3: Classification success rate for Full limb region for different camera view

Body Part	Camera View	Color Normalization	Success Rate	Sensitivity	Specificity
Full Limb	Anterior	Original	70.00%	100.00%	40.00%
		Lum	70.00%	80.00%	71.43%
		NormGrey	90.00%	100.00%	80.00%
		NormRGB	90.00%	80.00%	100.00%
		NormRGB-lum	90.00%	100.00%	80.00%
	Lateral	Original	72.72%	68.75%	76.47%
		Lum	72.72%	68.75%	76.47%
		NormGrey	78.78%	75.00%	82.35%
		NormRGB	72.72%	81.25%	64.71%
		NormRGB-lum	75.75%	75.00%	76.47%

Table 4 : Features, data normalization and pattern classification methods used for best classification for full limb region.

Body Part	Camera View	Color Normalization	Features	Data Normalization	Pattern Classification
Full Limb	Anterior	Original	Texture Correlation Histogram Energy	None	NN
		Lum	Histogram Energy	Soft-max, r = l	NN
		NormGrey	Spectral Histogram StdDev	Soft-max, r = l	NN
		NormRGB	Spectral Texture Inertia Histogram StdDev Histogram Energy Histogram Entropy	Standard Normal	NN
		NormRGB-lum	Spectral Histogram StdDev	Soft-max, r = l	NN
	Lateral	Original	Texture Correlation	Soft-max, r = l	NN
		Lum	Texture Correlation	Soft-max, r = l	NN
		NormGrey	Texture InvDiff Histogram StdDev Histogram Skew Histogram Entropy	Soft-max, r = l	NN
		NormRGB	Texture Energy Texture Correlation	Standard Normal	KNN5
		NormRGB-lum	Histogram Mean Histogram StdDev Histogram Skew Histogram Energy	Soft-max, r = l	NN

Table 5: Classification success rate for Shoulder/Hip for different camera view

Body Part	Camera View	Color Normalization	Success Rate	Sensitivity	Specificity
Shoulder/Hip	Lateral	Original	65.00%	50.00%	80.00%
		Lum	72.5%	80.00%	65.00%
		NormGrey	65.00%	70.00%	60.00%
		NormRGB	65.00%	55.00%	75.00%
		NormRGB-lum	67.50%	70.00%	65.00%

Table 6: Features, data normalization and pattern classification methods used for best classification for shoulder/hip region.

Body Part	Camera View	Color Normalization	Features	Data Normalization	Pattern Classification
Shoulder/Hip	Lateral	Original	Texture Inertia Texture InvDiff Histogram StdDev Histogram Skew Histogram Energy Histogram Entropy	Standard Normal	KNN5
		Lum	Texture Inertia Histogram Skew	Soft-max, r = l	KNN5
		NormGrey	Texture InvDiff Texture Entropy	Soft-max, r = l	KNN5
		NormRGB	Histogram Skew	Soft-max, r = l	NN
		NormRGB-lum	Texture Inertia Histogram Skew	Soft-max, r = l	NN

Table 7: Classification success rate for Wrist for different camera view

Body Part	Camera View	Color Normalization	Success Rate	Sensitivity	Specificity
Wrist	Anterior	Original	73.91%	75.00%	72.30%
		Lum	82.60%	91.67%	72.73%
		NormGrey	78.26%	83.33%	72.73%
		NormRGB	78.26%	83.33%	72.73%
		NormRGB-lum	82.60%	91.67%	72.73%
	Lateral	Original	79.31%	86.67%	71.43%
		Lum	79.31%	93.33%	64.29%
		NormGrey	75.86%	73.33%	78.57%
		NormRGB	68.96%	66.67%	71.43%
		NormRGB-lum	75.86%	86.67%	64.29%
	Posterior	Original	93.33%	100.00%	87.00%
		Lum	93.33%	100.00%	87.5%
		NormGrey	80.00%	85.71%	75.00%
		NormRGB	86.66%	100.00%	75.00%
		NormRGB-lum	93.33%	85.71%	100.00%

Table 8 : Features, data normalization and pattern classification methods used for best classification for wrist region.

Body Part	Camera View	Color Normalization	Features	Data Normalization	Pattern Classification
Wrist	Anterior	Original	Texture InvDiff Histogram Energy	None	NN
		Lum	Texture Energy Texture Entropy Histogram Mean	Soft-max, r = l	NN
		NormGrey	Texture Correlation Texture Entropy Histogram Skew	Standard Normal	NN
		NormRGB	Spectral Histogram StdDev Histogram Entropy	Standard Normal	NN
		NormRGB-lum	Histogram Mean Histogram StdDev	None	NN
	Lateral	Original	Texture Correlation Texture InvDiff Texture Entropy Histogram Entropy	Soft-max, r = l	KNN5
		Lum	Texture Entropy Histogram Mean	Standard Normal	KNN5
		NormGrey	Texture InvDiff	None	NN
		NormRGB	Texture Inertia Texture Entropy	Soft-max, r = l	KNN5
		NormRGB-lum	Texture Energy Texture Entropy Histogram Mean	Standard Normal	NN
		Original	Texture Inertia Texture Correlation Texture InvDiff	Soft-max, r = l	NN

Wrist	Posterior		Texture Entropy		
		Lum	Texture Correlation Histogram Entropy	None	NN
		NormGrey	Texture InvDiff	Soft-max, r = l	NN
		NormRGB	Texture InvDiff Texture Entropy Histogram mean Histogram StdDev	Soft-max, r = l	NN
		NormRGB-lum	Histogram Mean Histogram StdDev	Soft-max, r = l	NN

Table 9: Best classification results for different body parts.

Body Part	**Camera View**	**Color Normalization**	**Success Rate**	**Sensitivity**	**Specificity**
Elbow Knee	Anterior	normRGB-lum	85.36%	85.00%	85.71%
Full Limb	Anterior	normRGB-lum	90.00%	100.00%	80.00%
Shoulder/Hip	Lateral	lum	72.5%	80.00%	65.00%
Wrist	Posterior	lum	93.33%	100.00%	87.5%